CHAPTER 3

PETROGRAPHY AND CLAY MINERALOGY

3.1. Introduction

X-ray diffraction analysis is an indispensible tool in analytical sedimentology, especially for clay mineral analysis of shale and sandstone cement (Klung and Alexander, 1974). XRD is the diffraction of a beam X-rays of very short wave-length radiation in the 0.1 – 100°A interval by the three dimensional periodic array of atoms in a crystal (Zimmerle, 1995).

The (XRD) method of clay mineral analysis was carried out on shales, mudstone, and metasediments samples. The purpose of the analysis is to study the clay minerals present in these rock samples, and their distribution throughout the study area.

The clay minerals present can be used to infer the depositional environment of the shale and mudstone units. The samples preparation is given in Appendix A (method practised in the Geology Dept. University of Malaya) and the detail results are presented as below.

3.2. Field Observations and Samples Description

The main objective of this part is to introduce a general description of the carbonaceous rock units and handspecimen samples used in this study.

3.2.1. Semantan Fm. Samples

Generally the Semantan Formation as proposed by Jaafar bin Ahmad (1976) consist mainly of thinly and thickly bedded tuffaceous sandstone and interbedded mudstone and shale. The tuffaceous sandstone is well-bedded greyish orange color

and it occur with sharp plane top and basal contact with the alternating mudstone-shale beds. The tuffaceous sandstone exhibits parallel and convolute lamination. Thick bedded tuffaceous sandstone show graded bedding 'Bouma sequence'. The carbonaceous materials form thin layers interbedded with the tuffaceous sandstone. Graded tuffaceous sandstone show sharp interface between the sandstone and mudstone. (Plates 3.1, 3.2a, 3.2b). The black shale beds have sharp contact, and is made up of silt size grains and fine sand size grains. Parallel laminations are also common in the black shale.

3.2.2. Permian Sequence Samples

The Permian sequence is well exposed at Jengka Pass (Figure 2.1b). The sequence consist of folded and faulted beds of thinly bedded bituminous bioclastic limestone, black shale and tuffaceous sandstone. The limestone is rich in fossil assemblage and is black due to the abandance of organic matter, it is hard, with small joints and fractures (filled with secondary calcite veins) distributed randomly (Plate 3.3). The black shale have silt-sized and fine sand size grains. The shale show fissility and in some samples exhibit brown remenent signs of plant (peat) parallel to bedding planes of lamination (Plate 3.4). The black shale are preserved with parallel lamination in the order of 1 mm and consists of alternation of dark and light color (Plate 3.5).

3.2.3. Charu Samples

The name of the Charu Formation retained and formalized by Metcalfe et al., (1980), is derived from the Sungai Charu geographic locality. According to the same authors the Charu Fm. is conformably overlain by the Panching Limestone. The base

Plate 3.1. Handspecimen show sharp contact between tuffaceous sandstone and alternating shale-mudstone beds. Semantan Formation.

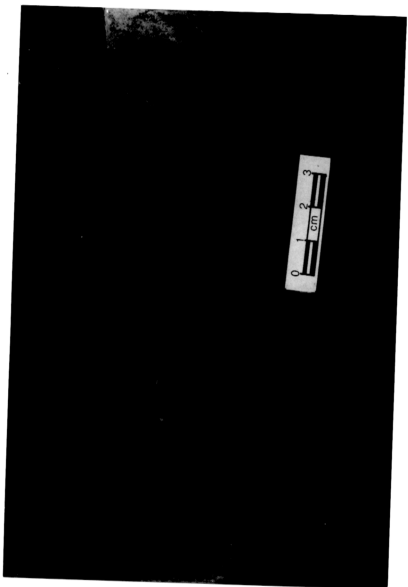

Plate 3.2a. Graded tuffaceous sandstone handspecimen note: the occasional grey mudstone layers and sharp interface between the sandstone and mudstone "Semantan Formation".

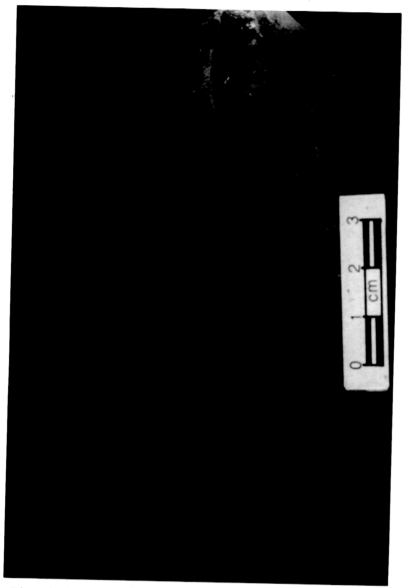

Plate 3.2b Tuffaceous sandstone show layer of mudstone (Semantan Formation)

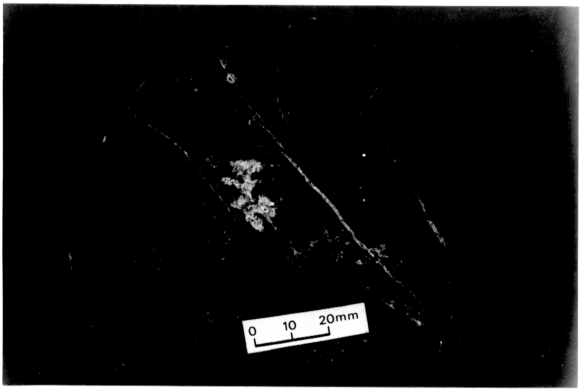

Plate 3.3. Permian Limestoen hand specimen show small joints and fracture distributed randomly filled with secondary calcite. "Jengka Pass".

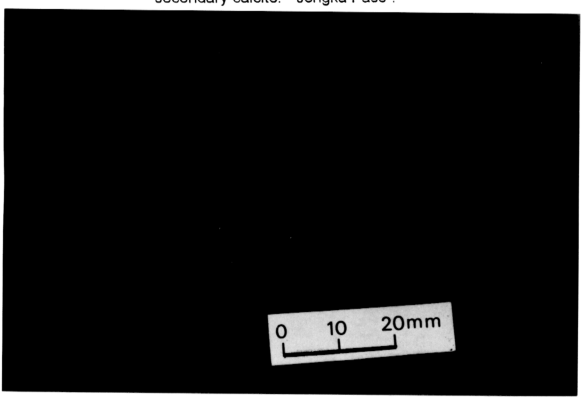

Plate 3.4. Cabocanceous shale hand specimen illustrate plant remains Permian Formation.
Location: Jengka Pass.

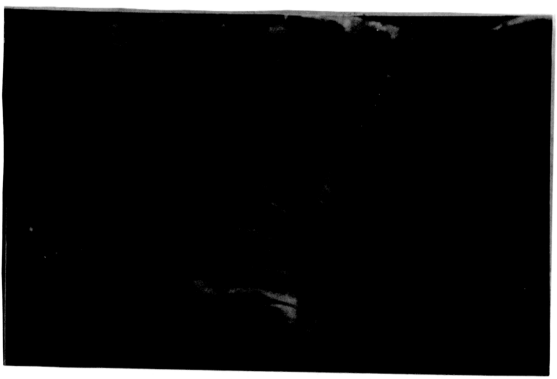

Plate 3.5. Black shale show lamination with alternation dark and light color. Permian sequence at Jengka Pass.

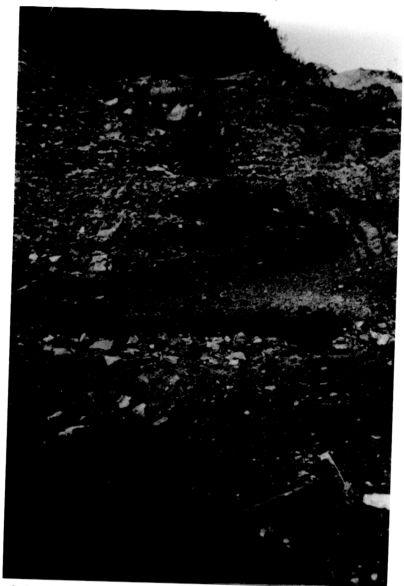

Plate 3.6. Weathered black shale of Charu Formation which change to friable soil (28 km to Kuantan town).

of this formation right now is not exposed and the nature of the underlying strata is unknown. The estimated thickness of this formation as reported by Metcalfe et. al., (1980) is approximately 1600 m. The Charu Formation consists of interbedded sandstone, shale and siltstone. They are well exposed along road cuts from 28 km to Kuantan town. The sandstone is medium grained and grades up sequence up into siltstone.

The sandstone beds range in thickness from 1 meter to 3 meters and the color appear to be from greyish-white to orange-yellow. The siltstone beds occur in thin beds, and it's thickness range from 80 to 90 cm. The color of the siltstone beds range from greyish to red. Both siltstone and sandstone beds show primary sedimentary structure of ripple mark, grading and cross bedding.

Carbonaceous shale is the most abundant rock unit in this formation. The shale beds exhibit fissile character and in black color due to the abundance of carbonaceous matter. The highly weathered part change to friable soil (Plate 3.6). The lower part of the shale exhibit two beds of coaly shale with thickness range from 70 to 80 cm (Plates 3.7, 3.8). The laminations of carbonaceous sediments are generally in the order of 1 mm and consist of alternation of dark and light layers. The lighter layers are of silt and fine sand, while the dark color layers are of clay size particles with carbonaceous matter (Plate 3.9).

3.2.4. Panching Limestone Samples

Metcalfe, et al., (1980) formalised and retained the name Panching Limestone which is derived from Bt. Panching situated near Panching village. The outcrops are composed of four limestone hills namely Bt. Panching, Bt. Charas, Bt. Sagor, and

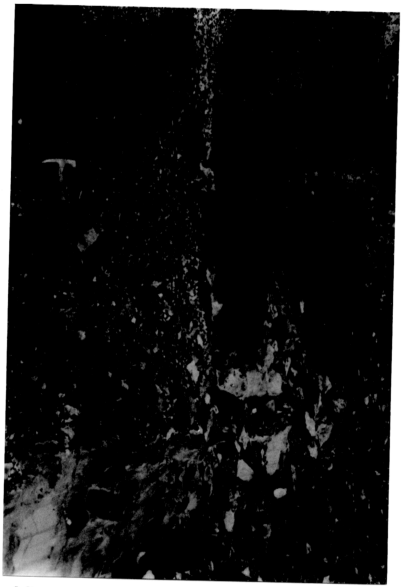

Plate 3.7. Black shale in Charu Formation show thinly beds of coaly shale (28 km to Kuantan town).

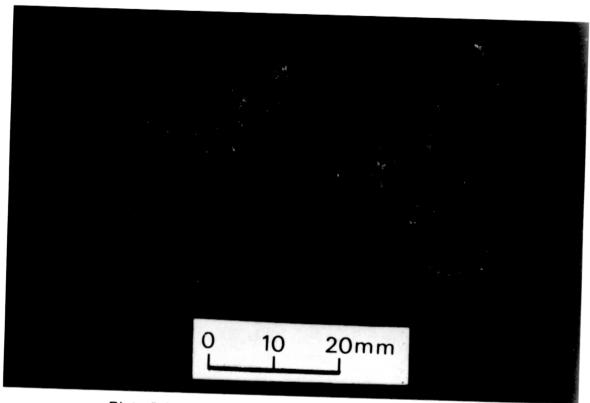

Plate 3.8. Coaly shale handspecimen from Charu Formation. "Sampel Ch_4, 28 km to Kuantan".

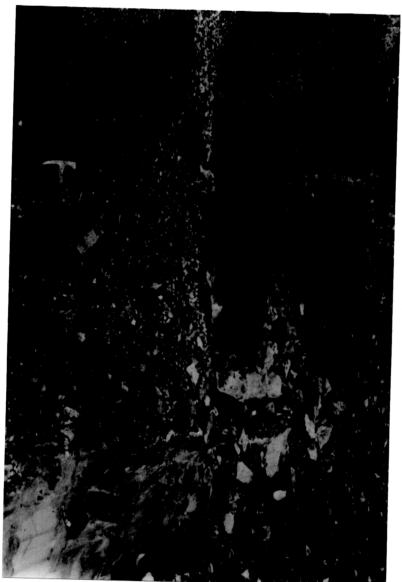

Plate 3.9. Black shale in Charu Formation show dark and light lamination.
Location: (28 km to Kuantan town).

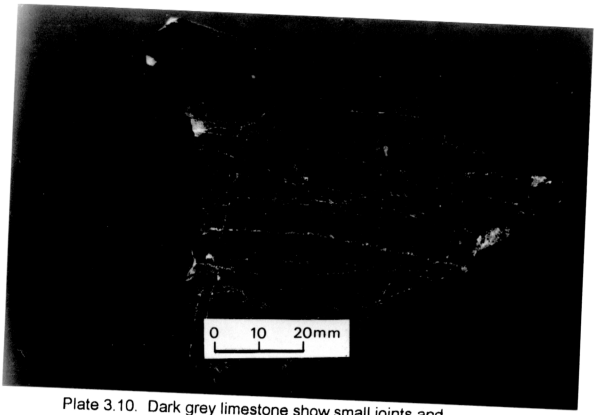

Plate 3.10. Dark grey limestone show small joints and fracture distributed randomly, filled with secondary calcite. (Sample Pa_1, Bt. Panching)

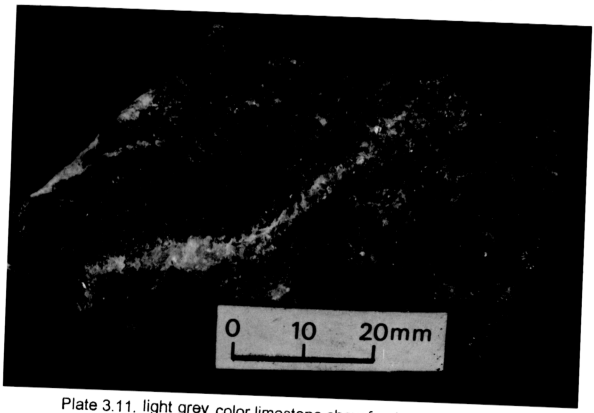

Plate 3.11. light grey color limestone show fracture filled with secondary calcite, bottom side right red color due to weathering of hematite grains (Sample Pa_2 Bt. Panching).

Bt. Tenggek. The limestone in Bt. Panching now is being quarried. The Panching Limestone lies conformably over the older Charu Formation Tan (1972). The maximum thickness of the limestone is of approximately 600 meters (Metcalfe, et. al., 1980).

The limestone consists of sequences of massive bedded, recrystallized limestone, fossiliferous, it's color ranging from light grey to dark grey due to change of organic matter concentration in rock units, hard, small joints and fractures distributed randomly filled with secondary calcite veins. Also huge calcite veins forming rhombohedral cleavages have been observed.

Plates 3.10, 3.11 are photos of hand specimen from the Panching Limestone hill. The speciments range from light grey to dark grey in colour, fossiliferous, crystalline in texture and cut by numerous small calcite veins. Irregular small holes due to erosional and solution effect are also observed. Secondary iron oxides occurred on the surface of limestone. The presence of the hematite grains could be related to the accumulation of iron-oxide rich solution perculating through fractures and joints plane.

3.2.5. Sagor Samples

In general the name of the Sagor Formation retained and formalized by Metcalfe et. al., (1980). It was chosen from Bt. Pak Sagor geographic locality. The rocks described in this study are exposed in Bt. Pak Sagor. Tan (1972) said the Sagor beds conformably overlying the Panching Limestone. This formation has a maximum thickness approximately 1500 m (Metcalfe, et. al., 1980). The Sagor Formation

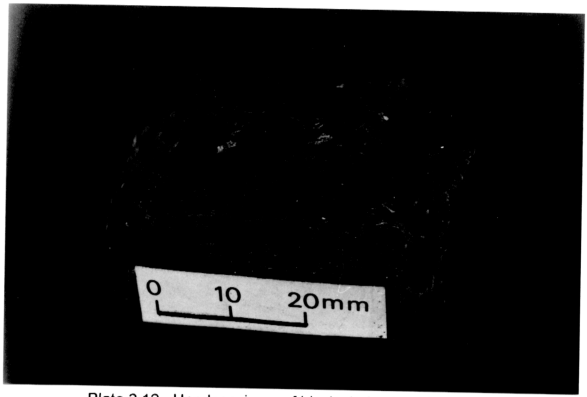

Plate 3.12. Handspecimen of black shale show fissility (Sample Sa_2, Bt. Sagor).

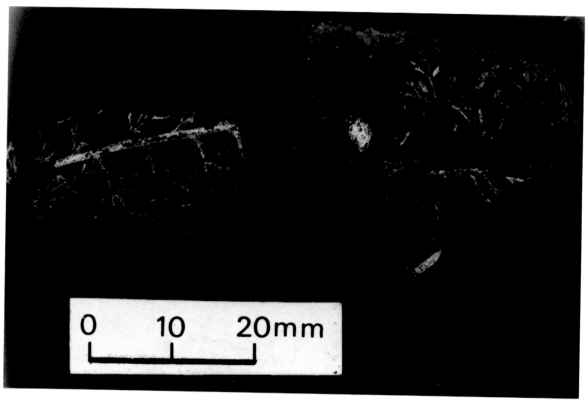

Plate 3.13. Plant leaf fragment preserved between bedding planes of the carbonaceous shale (Sample Sa_4, Bt. Pak Sagor).

lithologically consist of sandstone, shale and mudstone. Tan (1972) and Metcalfe et. al., (1980) described the presence of conglomerate beds at the base of the formation in the Bt. Pak Sagor, the reported conglomerate may be indicate that the deposition environment in the lower part of this formation was of higher energy regime.

The sandstone occurs as interbeds with thin shale or mudstone. The carbonaceous lamination in the form of lenticular streaks sub parallel to one another is also present in shales. Primary sedimentary structure such as graded bedding have been seen in some sandstones. Fine wavy lamination of silty layer parallel to the bedding occur in thinly interbedded shale and mudstone. Fissility also occur in black shale (Plate 3.12). Plant remains parallel to the bedding planes of lamination have been observed in some samples of the Sagor Formation (Plate 3.13).

3.2.6. Kemaman (Chukai) Metasediments Samples

At the Kemaman, Chukai area the sandstone and carbonaceous shale were subjected to a regional metamorphism producing metasediments sequence of greyish metaquartzite, carbonaceous slate and phyllite. Most of the samples in this study have been taken from and around Bt. Tg Mat Amin (Plate 3.14). The sequence of this area is consist of metaquartzite carbonaceous slate and phyllite. The metaquartize is composed predominently of quartz. The quartz is greyish in color, medium to fine grains. Primary sedimentary structures such as cross-bedding of small scale type, lamination, and graded bedding are well preserved in this type of rock units. The greyish color could be related to the perculation of solution rich in organic matter staining the cement meterials of the sandstone. Secondary sedimentary structure of quartz veins are frequently found cutting the metaquartzite.

The slate is black due to the predominance of organic matter, relatively hard,

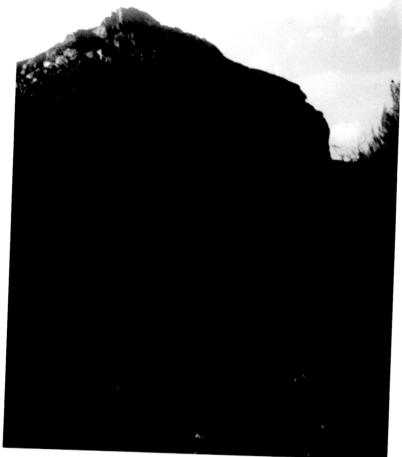

Plate 3.14. Photograph of Bt. Tg. Mat Amin (Chukai).

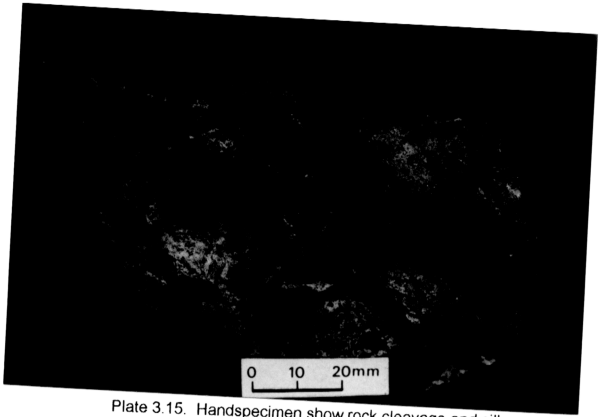

Plate 3.15. Handspecimen show rock cleavage and silky sheen in black slate. (Sample Km_3 Bt. Tg. Mat Amin).

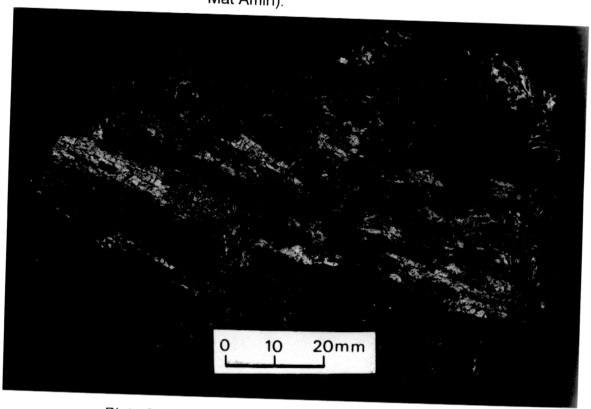

Plate 3.16. Phyllite show masked luster due to high content of carbon in the form of graphite. Note foliation (Sample Km_4 Bt. Tg. Mat Amin).

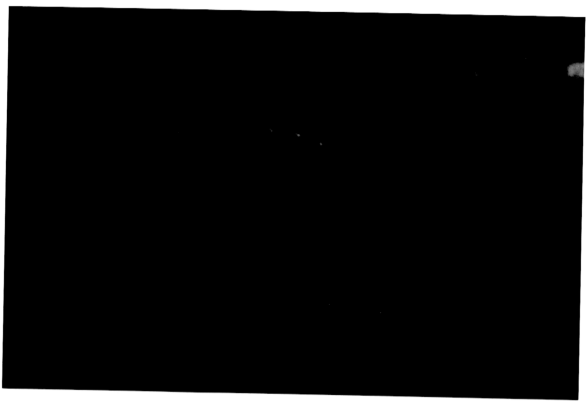

Plate 3.17. Photograph show repeatation of strata by folding Bt. Tg. Mat Amin (Chukai).

and show well developed slaty cleavage. The cleavage surface of the slate illustrate a sheen (Plate 3.15).

The phyllite is pitch black in color, weathered samples easily change to soil when rubbed by fingers. The high content of carbon in the form of graphite masked the luster sheen of the phyllite (Plate 3.16). In this area repeatation of strata by folding have been observed in Bt. Tg. Mat Amin outcrop (Plate 3.17)

3.3. Clay Minerals Investigations

The objective of the investigation is to identify clay minerals present in the study area. The analysis were made by X-ray diffraction techniques by using a diffractometer Philips PW 2243/20, Cu Kα and Ni filter.

X-ray diffractograms show illite and kaolinite are the most abundant clay minerals in all the samples studied (Figures 3.1A, 3.1B, 3.1C, 3.1D, 3.1E and 3.1F).

3.4. Clay Mineralogy

The clay minerals present in this study and its distribution throughout the sediments of the area understudy are presented in Table 3.1.

3.4.1 Illite

Illite was observed in almost every sample studied, it was recognized by their strong first and third order basal reflections respectively. The (001) reflection at 8.8 2°0 10A° and the (003) reflection at 26.6 20° 3.3A°. The later reflection may be coincides with strongest quartz reflection if quartz occurs in the clay fraction (see diffractograms and tables).

Table 3.1 Distribution of clay minerals in the sediments studied.

Locality	Sample	Lithology	Illite	Kaolinite	Chlorite	Pyrophyllite
Charu Fm	Ch1	Shale	x	x		
	Ch2	Coalyshale	x	x		
	Ch3	Shale	x	x		
	Ch4	Coalyshale	x	x		
	Ch5	Shale	x	x		
Sagor Fm	Sa1	Shale	x	x		
	Sa2	Shale	x	x		
	Sa3	Shale	x	x		
	Sa4	Shale	x	x		
Permian Sequence	Per1	Shale	x	x		
	Per2	Shale	x	x		
	Per3	Shale	x	x		
	Per4	Shale	x	x		
Semantan Fm	Tr1	Shale	x	x		
	Tr2	Shale	x	x		
Kemaman Cukai metasediment	Km 1	Phyllite	x	x	x	x
	Km 2	Phyllite	x	x	x	x
	Km 3	Slate	x	x	x	x
	Km 4	Phyllite	x	x	x	x
	Km 5	Slate	x	x	x	x
	Km 6	Slate	x	x	x	x
	Km 7	Slate	x	x	x	x
	Km 8	Slate	x	x	x	x
	Km 9	Slate	x	x	x	x
	Km 10	Slate	x	x	x	x
	Km 11	Slate	x	x	x	x
	Km 12	Slate	x	x	x	x

Both bulk and clay sized fraction samples after treatment with ethylene glycol and heated at 350°C and 550°C. No changes occured on the basal spacing (Figures 3.3A, 3.3B, 3.3C, 3.3D, 3.3E, 3.3F). The lack of response of illite to both heating and glycolation implies that the interlayered positions are completely occupied by cations and that cations are about the same size as K^+ or larger (Barshad, 1950).

Illite is also recognized by the presence of the relatively sharp (002) basal reflections at 17.2 20° 5A°. The relatively sharp 5A° indicate dioctahedral illite and high ratio of iron content of octahedral layer. The behaviours of the basal reflection upon treatment are shown in Tables 3.2A, 3.2B, 3.2C, 3.2D. The X-ray diffractograms of samples denoted by Km_1 to Km_{13} Figures 3.1E, 3.1F display the (001) basal reflections at 10A° of the illite is partially overlapped by the (002) basal reflection of the pyrophillite at 9.5 2°0 9.3A° toward the high angle side of illite.

The SEM photographs (Plates 3.18a, 3.18b, 3.18c, 3.18d) for the samples Ch_4, Per_3, Tr_3, Sa_4, show massive detrital illite composed of irregular, flaky like clay platelets oriented parallel to each other. The flaky morphology of this detrital illite is not unique to illite, thus is of no help in identifying this clay, precise identification is based on X-ray diffraction (XRD) analysis and EDX analysis. The EDX analysis of illite (Figures 3.2a, 3.2b, 3.2c, 3.2d) yield the major elements: Si, Al and K, with a minor amounts of Mg, Ca and Fe. In the illite EDX spectrum, the relative peak height of K is usually less than of Al. This is in contrast to K-feldspars where the K and Al peaks are of equal height.

3.4.1.1.Crystallinity of Illite

The shape of the basal reflections of illite can be used to evaluate the crystallinity (Thorez, 1976). The shape of the basal reflections detected for the samples number Sa_4, Per_3, Tr_3, show the (001) basal reflections at 10A° is relatively narrow and symmetrical (Figures 3.1B, 3.1C, 3.1D). This is indicate that the mineral well crystallized.

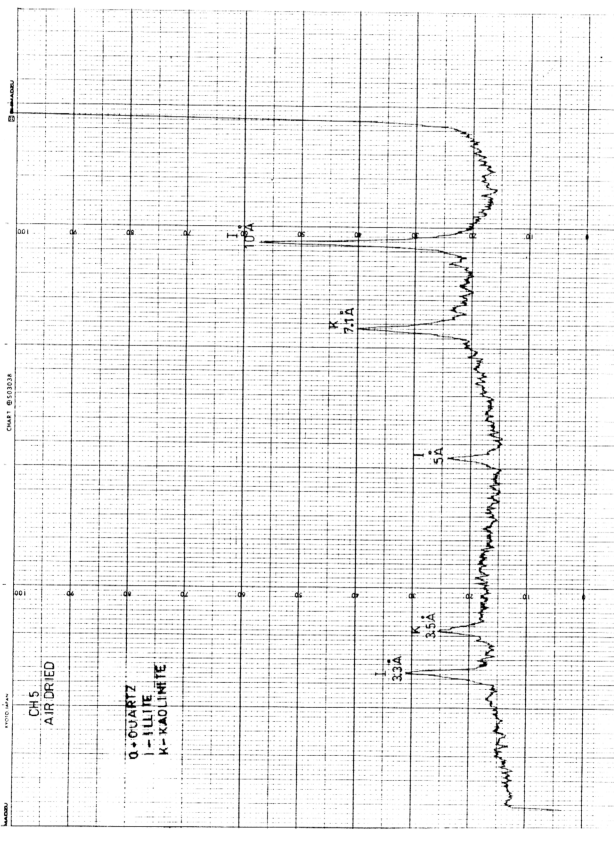

Figure 3.1A. X-ray diffraction pattern of untreated (sample Ch_5) <2 µm.

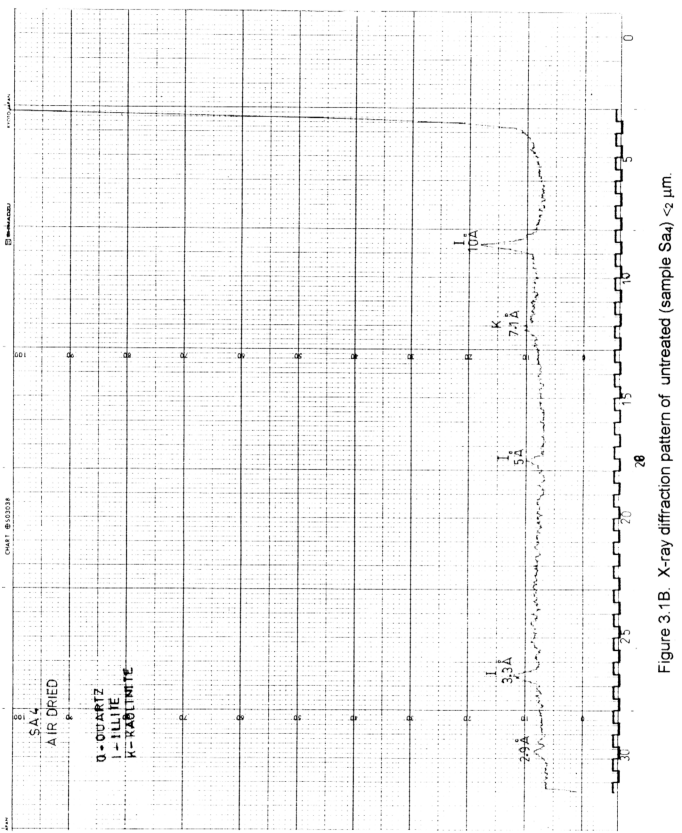

Figure 3.1B. X-ray diffraction pattern of untreated (sample Sa_4) <2 µm.

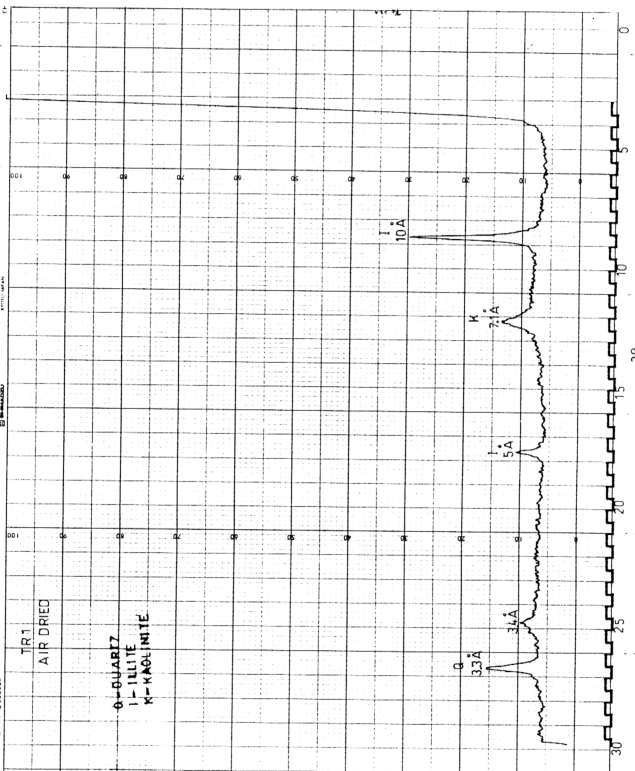

Figure 3.10: X-ray diffraction pattern of [illegible]

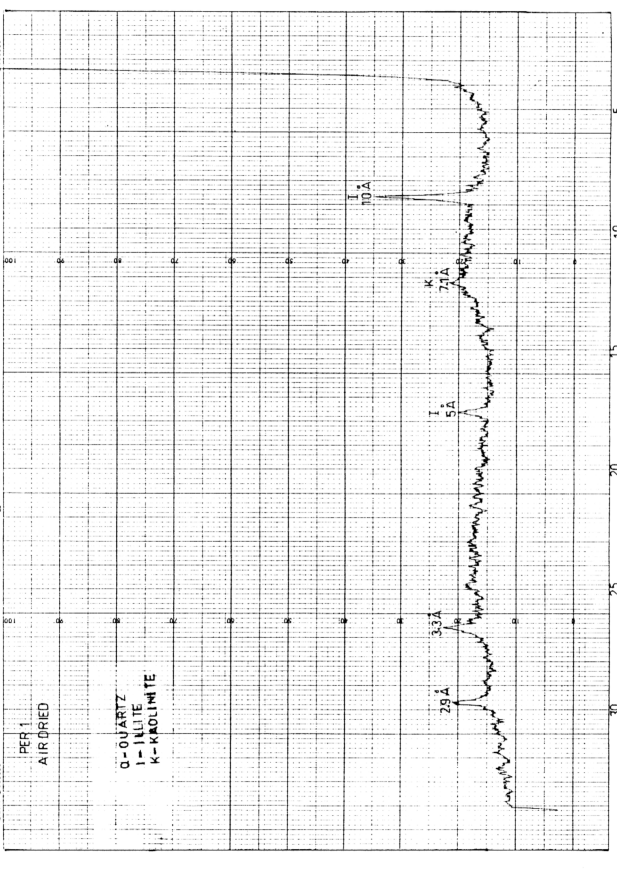

Figure 3.1D. X-ray diffraction pattern of untreated (sample Per_1) $< 2\ \mu m$.

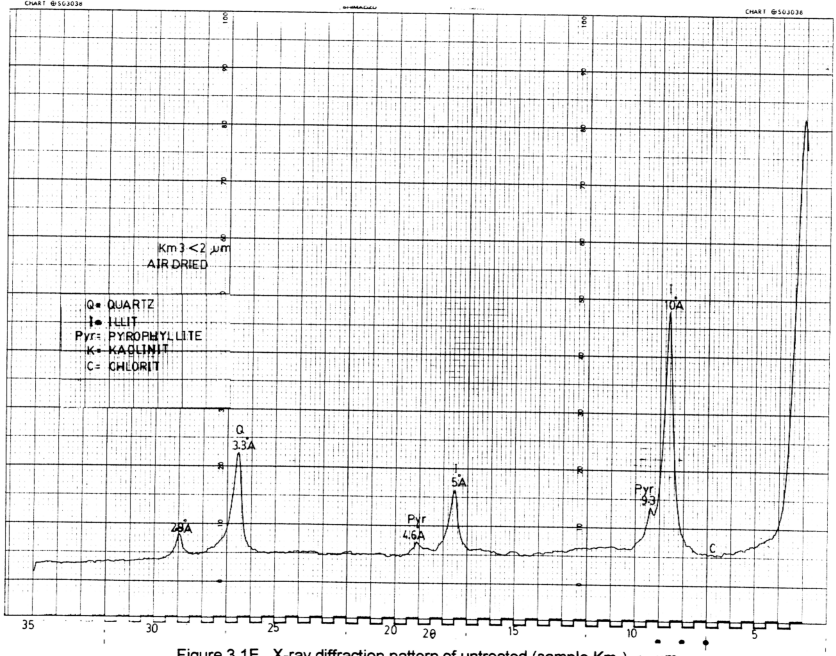

Figure 3.1E. X-ray diffraction pattern of untreated (sample Km_3) < 2 µm.

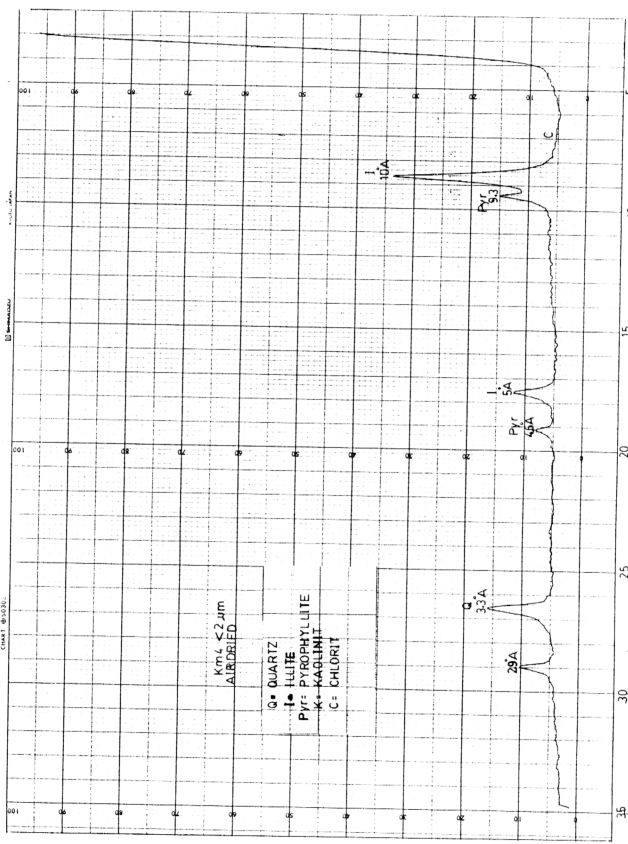

Figure 3.1F. X-ray diffraction pattern of untreated (sample Km_4) <2 µm.

Table 3.2A. The behaviour of basal reflections of illite upon treatments (bulk analysis).

Sample No.	(001)				(002)				(003)			
	N	Treatments			N	Treatments			N	Treatments		
		GE	350°	550°C		GE	350°C	550°C		GE	350°C	550°C
Ch_1	10 A°	No changes			5 A°	No changes			3.3 A°	No changes		
Ch_2	10 A°	~	~	~	5 A°	~	~	~	3.3 A°	~	~	~
Ch_3	10 A°	~	~	~	5 A°	~	~	~	3.3 A°	~	~	~
Ch_4	10 A°	~	~	~	5 A°	~	~	~	3.3 A°	~	~	~
Ch_5	10 A°	~	~	~	5 A°	~	~	~	3.3 A°	~	~	~
Sa_1	10 A°	~	~	~	5 A°	~	~	~	3.3 A°	~	~	~
Sa_2	10 A°	~	~	~	5 A°	~	~	~	3.3 A°	~	~	~
Sa_3	10 A°	~	~	~	5 A°	~	~	~	3.3 A°	~	~	~
Sa_4	10 A°	~	~	~	5 A°	~	~	~	3.3 A°	~	~	~
Pe_{r1}	10 A°	~	~	~	5 A°	~	~	~	3.3 A°	~	~	~
Pe_{r2}	10 A°	~	~	~	5 A°	~	~	~	3.3 A°	~	~	~
Per_3	10 A°	~	~	~	5 A°	~	~	~	3.3 A°	~	~	~
Tr_1	10 A°	~	~	~	5 A°	~	~	~	3.3 A°	~	~	~
Tr_2	10 A°	~	~	~	5 A°	~	~	~	3.3 A°	~		~

N - normal (air dried sample); GE = Glycol ethylene

Table 3.2B. The behaviour of basal reflections of illite upon treatments <2 μm factions

Sample No.	(001)				(002)				(003)			
		Treatments				Treatments				Treatments		
	N	GE	350°	550°C	N	GE	350°C	550°C	N	GE	350°C	550°C
Ch_1	10 A°	No changes			5 A°	No changes			3.3 A°	No changes		
Ch_2	10 A°	~	~	~	5 A°	~	~	~	3.3 A°	~	~	~
Ch_3	10 A°	~	~	~	5 A°	~	~	~	3.3 A°	~	~	~
Ch_4	10 A°	~	~	~	5 A°	~	~	~	3.3 A°	~	~	~
Ch_5	10 A°	~	~	~	5 A°	~	~	~	3.3 A°	~	~	~
Sa_1	10 A°	~	~	~	5 A°	~	~	~	3.3 A°	~	~	~
Sa_2	10 A°	~	~	~	5 A°	~	~	~	3.3 A°	~	~	~
Sa_3	10 A°	~	~	~	5 A°	~	~	~	3.3 A°	~	~	~
Sa_4	10 A°	~	~	~	5 A°	~	~	~	3.3 A°	~	~	~
Pe_{r1}	10 A°	~	~	~	5 A°	~	~	~	3.3 A°	~	~	~
Pe_{r2}	10 A°	~	~	~	5 A°	~	~	~	3.3 A°	~	~	~
Per_3	10 A°	~	~	~	5 A°	~	~	~	3.3 A°	~	~	~
Tr_1	10 A°	~	~	~	5 A°	~	~	~	3.3 A°	~	~	~
Tr_2	10 A°	~	~	~	5 A°	~	~	~	3.3 A°	~		~

N - Air dried, GE - Glycol ethylene, ND - not detected

Table 3.2C. The behaviour of basal reflections of illite upon treatments (bulk analysis) of Kemaman samples.

Sample No.	(001)				(002)				(003)			
	N	Treatments			N	Treatments			N	Treatments		
		GE	350°	550°C		GE	350°C	550°C		GE	350°C	550°C
Km_1	10 A°	No changes			5 A°	No changes			3.3 A°	No changes		
Km_2	10 A°	~	~	~	5 A°	~	~	~	3.3 A°	~	~	~
Km_3	10 A°	~	~	~	5 A°	~	~	~	3.3 A°	~	~	~
Km_4	10 A°	~	~	~	5 A°	~	~	~	3.3 A°	~	~	~
Km_5	10 A°	~	~	~	5 A°	~	~	~	3.3 A°	~	~	~
Km_7	10 A°	~	~	~	5 A°	~	~	~	3.3 A°	~	~	~
Km_8	10 A°	~	~	~	5 A°	~	~	~	3.3 A°	~	~	~
Km_9	10 A°	~	~	~	5 A°	~	~	~	3.3 A°	~	~	~
Km_{10}	10 A°	~	~	~	5 A°	~	~	~	3.3 A°	~	~	~
Km_{11}	10 A°	~	~	~	5 A°	~	~	~	3.3 A°	~	~	~
Km_{12}	10 A°	~	~	~	5 A°	~	~	~	3.3 A°	~	~	~
Km_{13}	10 A°	~	~	~	5 A°	~	~	~	3.3 A°	~	~	~

N - Air dried; GE - Glycol ethylene

Table 3.2D. The behaviour of basal reflections of illite upon treatments <2 μm factions of Kemaman samples.

Sample No.	(001)				(002)				(003)			
		Treatments				Treatments				Treatments		
	N	GE	350°	550°C	N	GE	350°C	550°C	N	GE	350°C	550°C
Km_1	10 A°	No changes			5 A°	No changes			3.3 A°	No changes		
Km_2	10 A°	~	~	~	5 A°	~	~	~	3.3 A°	~	~	~
Km_3	10 A°	~	~	~	5 A°	~	~	~	3.3 A°	~	~	~
Km_4	10 A°	~	~	~	5 A°	~	~	~	3.3 A°	~	~	~
Km_5	10 A°	~	~	~	5 A°	~	~	~	3.3 A°	~	~	~
Km_7	10 A°	~	~	~	5 A°	~	~	~	3.3 A°	~	~	~
Km_8	10 A°	~	~	~	5 A°	~	~	~	3.3 A°	~	~	~
Km_9	10 A°	~	~	~	5 A°	~	~	~	3.3 A°	~	~	~
Km_{10}	10 A°	~	~	~	5 A°	~	~	~	3.3 A°	~	~	~
Km_{11}	10 A°	~	~	~	5 A°	~	~	~	3.3 A°	~	~	~
Km_{12}	10 A°	~	~	~	5 A°	~	~	~	3.3 A°	~	~	~
Km_{13}	10 A°	~	~	~	5 A°	~	~	~	3.3 A°	~	~	~

N - Air dried, GE; Glycolated.

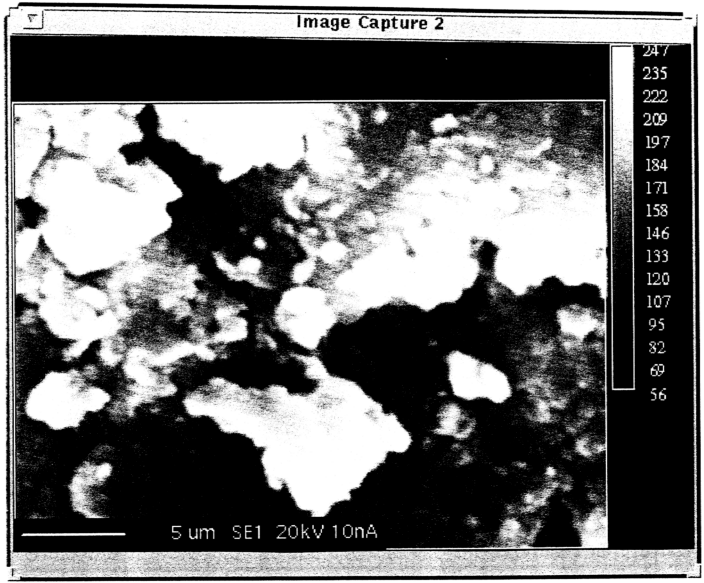

Plate 3.18A Scanning electron micrograph of (sample Ch₄)

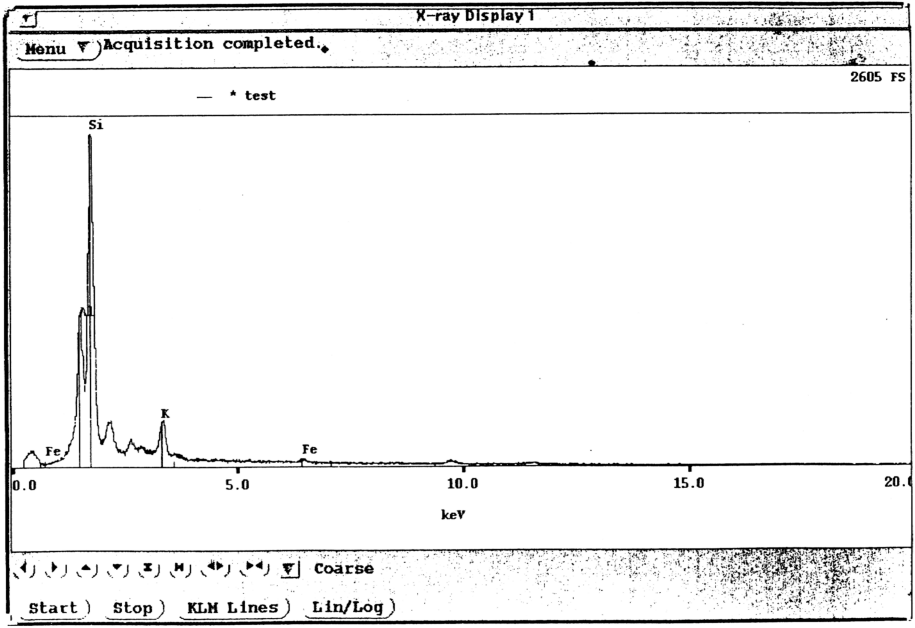

Figure 3.2A. Energy Dispersive X-ray spectrum (EDX) of illite (sample Ch_4).

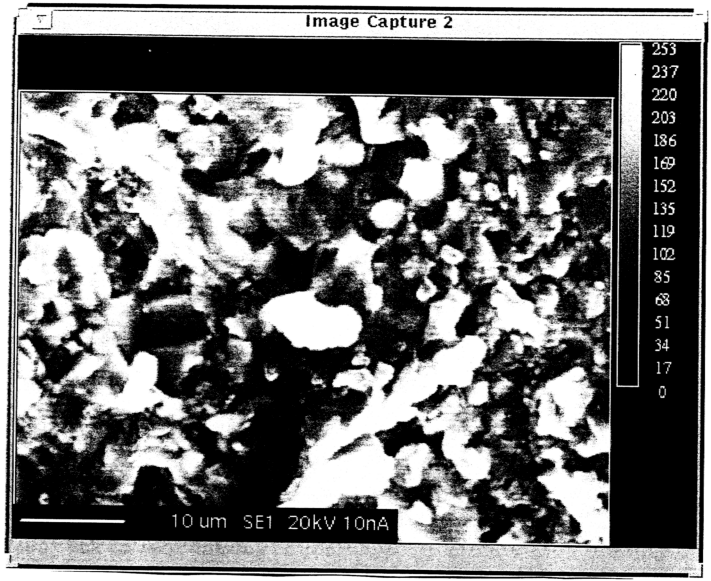

Plate 3.18B. Scanning electron micrograph. (sample Per_3) display flacky platelets illite.

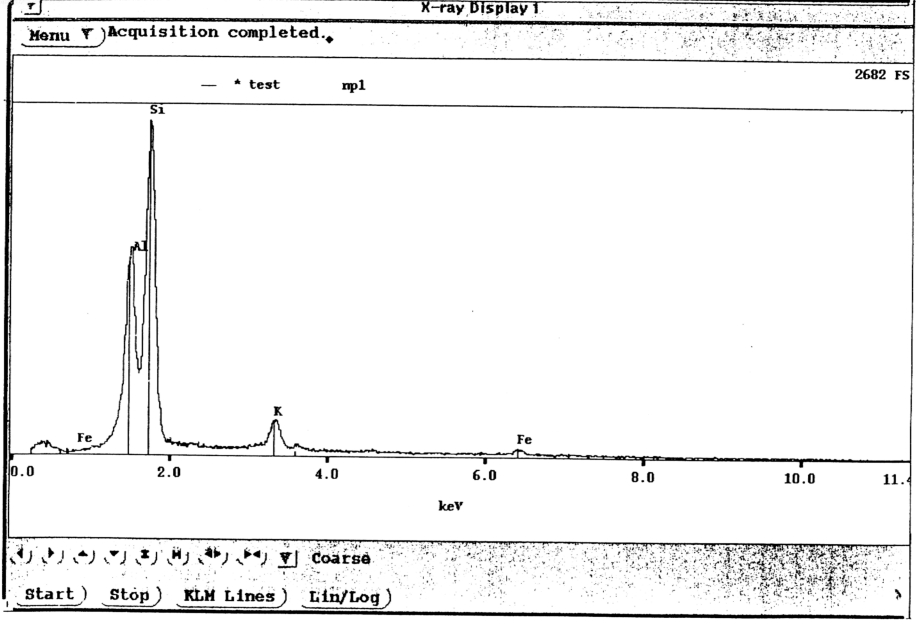

Figure 3.2B. Energy Dispersive X-ray spectrum (EDX) of illite (sample Per_3).

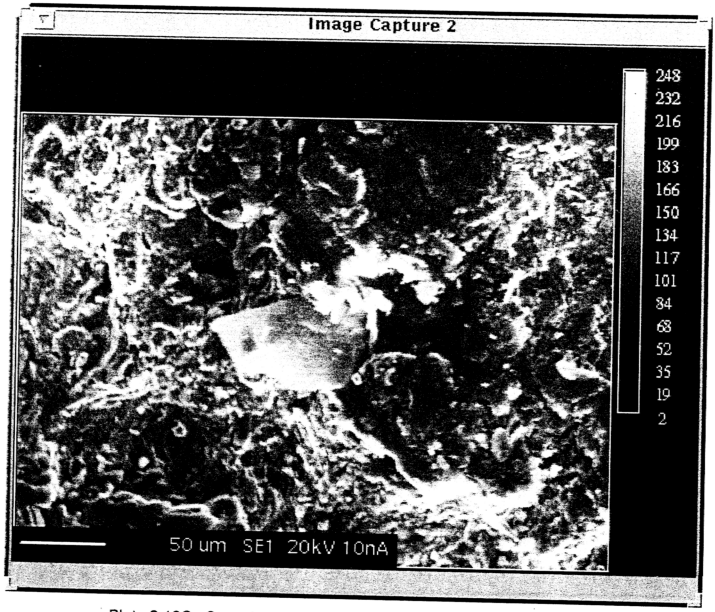

Plate 3.18C. Scanning electron micrograph of (sample Tr_3) show flacky platelets illite.

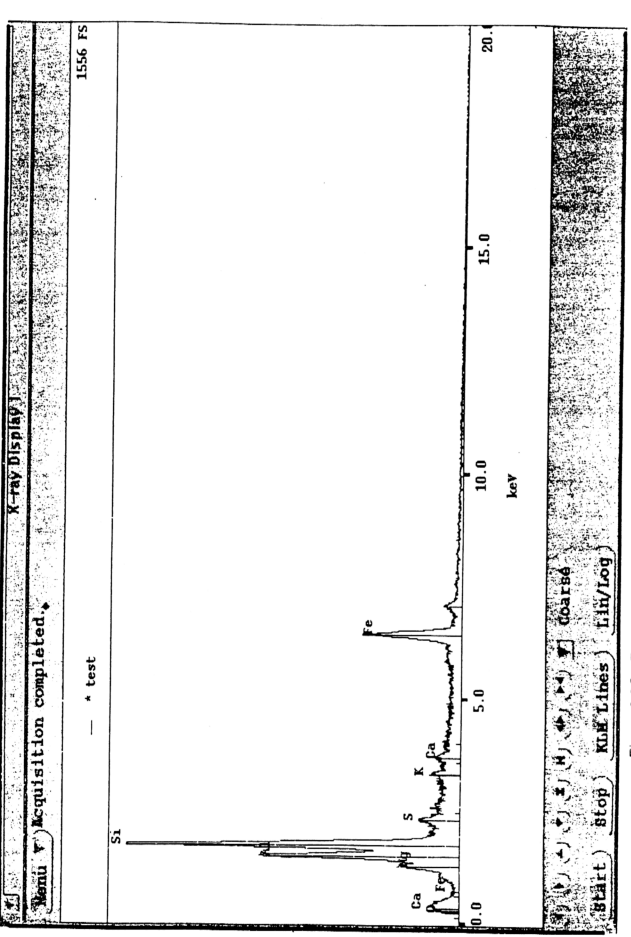

Figure 3.2C Energy Dispersive X-ray spectrum (EDX) of illite sample Tr_3.

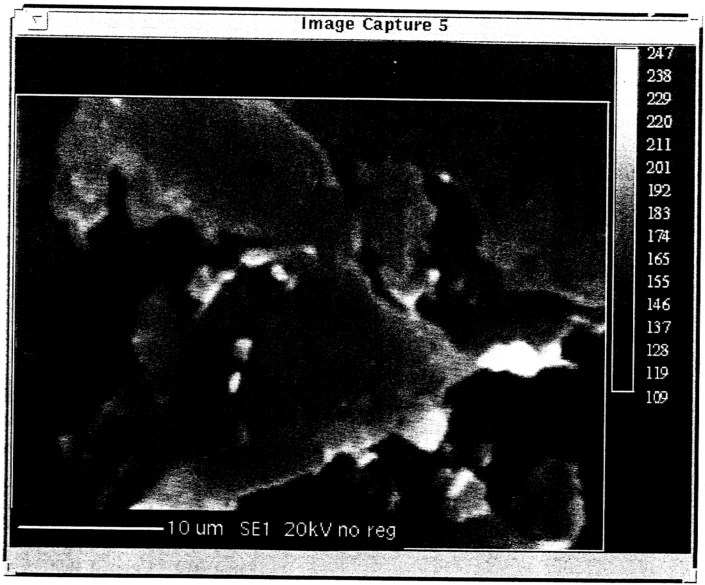

Plate 3.18D. Scanning electron micrograph of (sample Sa_4) show flacky platelets illite.

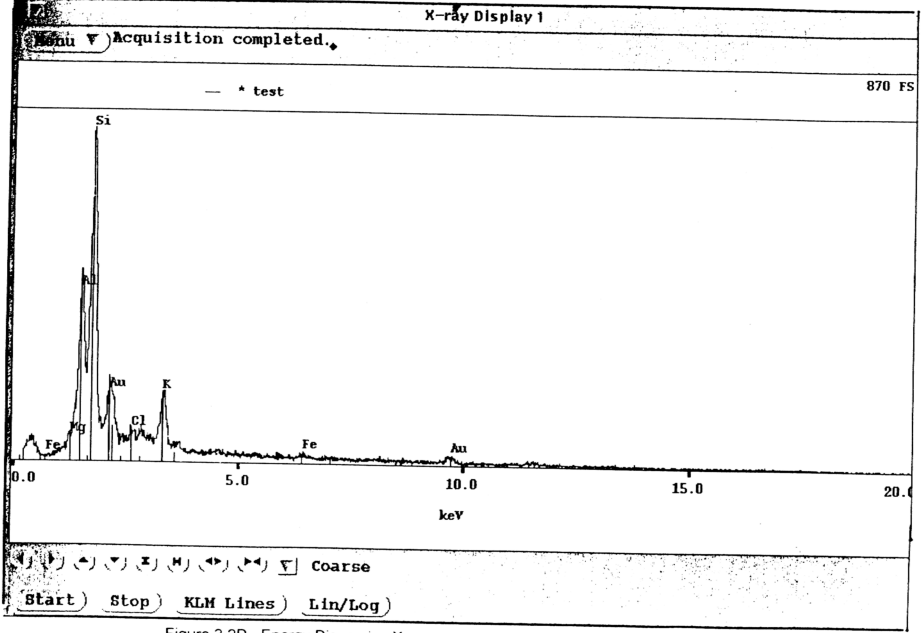

Figure 3.2D. Energy Dispersive X-ray spectrum (EDX) of illite (sample Sa_4).

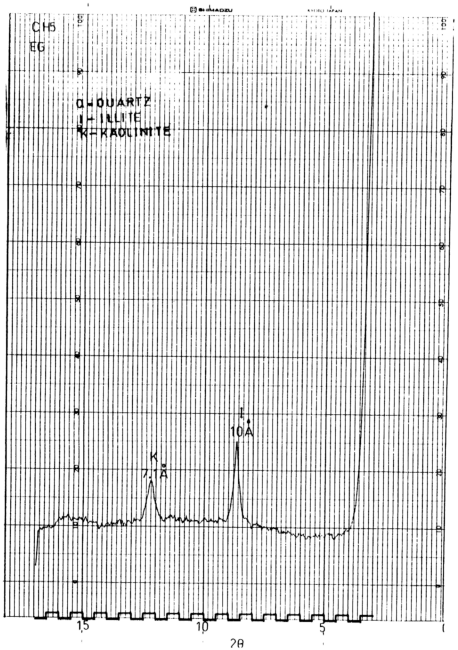

Figure 3.3A. X-ray diffraction pattern of sample Ch_5 after being glycolated.

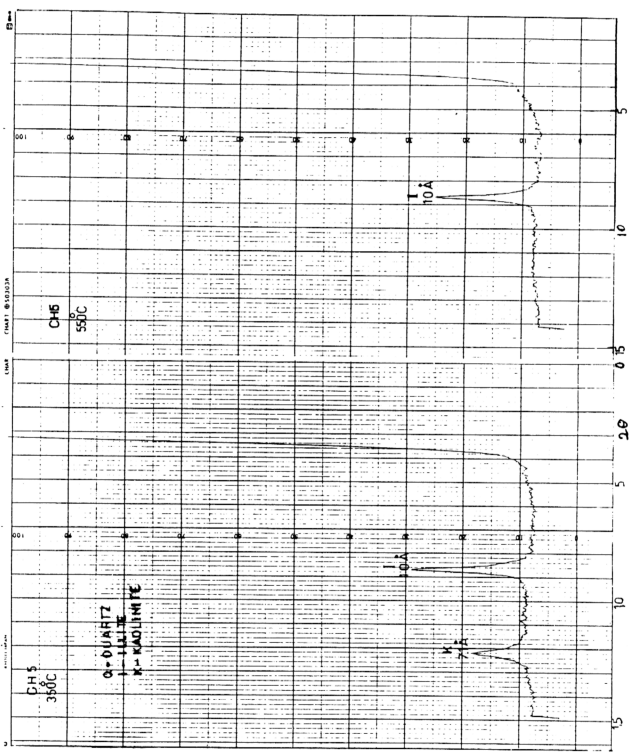

Figure 3.3B. X-ray diffraction pattern of sample Ch_5 after being heated.

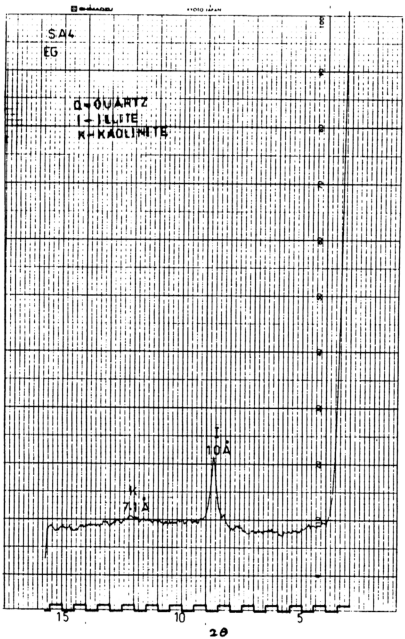

Figure 3.3C. X-ray diffraction pattern of sample Sa_4 after being glycolated.

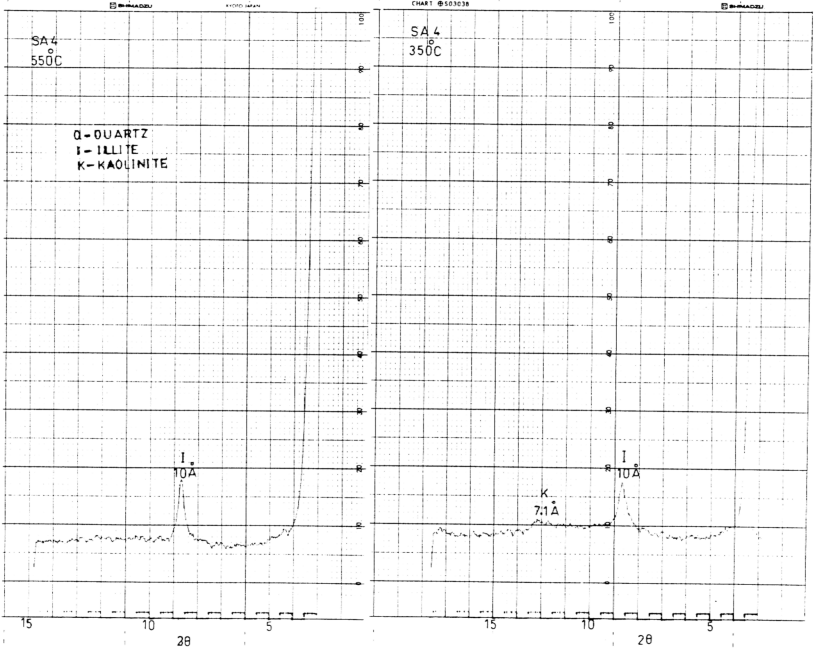

Figure 3.3D X-ray diffraction pattern of sample Sa_4 after being heated

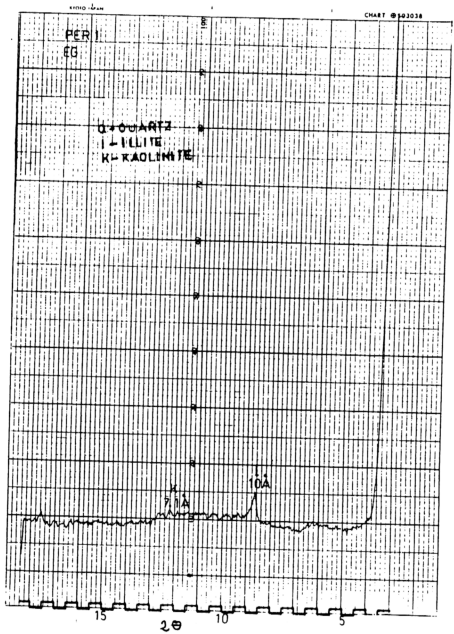

Figure 3.3E. X-ray diffraction pattern of sample Per_1 after being glycolated.

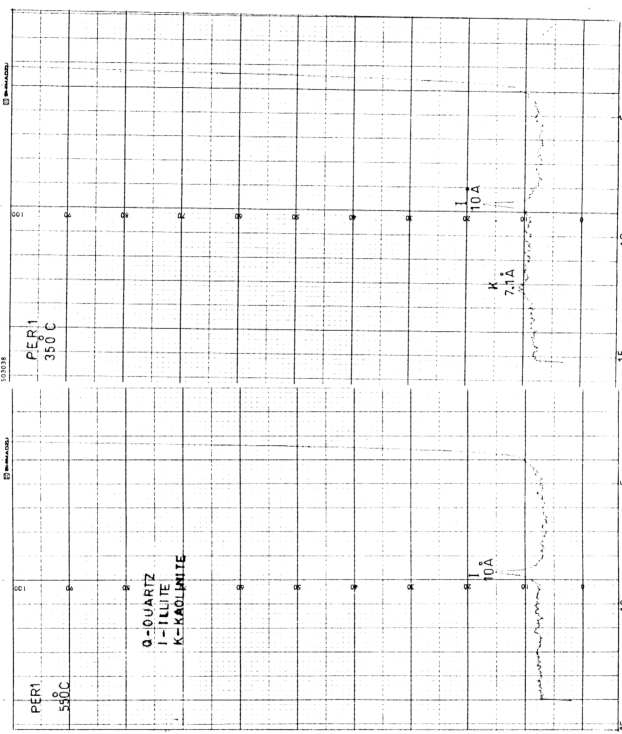

Figure 3.3F. X-ray diffraction of sample Per1 after being heated.

Sample number Ch5 show an asymmetry of the basal reflections at 10°A toward low angle side for (001) and toward high angle side for (003) while the (002) becomes broad (Figure 3.1A). This may be due to occurrence of a small amount of expansible layer instructure and corresponding to an open illite. The asymmetry also could be indicate of a transitional to mixed-layer system.

3.4.1.2. Crystallite Size Determination.

3.4.1.2.1. Introduction.

The technique of crystallite size determination by X-ray diffraction methods is based on the observed line width of the X-ray diffraction from sample and mean diameter of the crystallite in the sample. In general, X-ray methods are used to measure size in the submicron range. Kubler (1967), defined crystallinity as a degree of ordering in a crystalline lattice. Crystallinity usually signifies the amount of crystalline material in any substance (Frey, 1987).

The width of diffraction peaks from powder sample indicate the average size of the tiny crystall in analyzed specimen. Large crystall produce narrow peaks, small crystall produce broad, ill defined peaks (Griffin, 1971). Peak breadth measurements can yield a quantitative measure of the average dimensions of the cyrstallite producing the peak.

3.4.1.2.2. Measurement of Average Crystal Size of Illite

The following procedure has been used to determine crystallite size of illite minerals detected by X-ray diffraction for the samples used in this study. The results obtained and calculations are presented in Table 3.3.

1. One or more peaks for measurement have been selected.

2. The peaks should be symmetrical and unimodal with no interference from other neighboring peaks.
3. The dimension measured will be perpendicular to the planes producing the peak.
4. A basal (001) reflections peaks should be selected.
5. A base line perpendicular to the peaks apex have been constructed at point midway between the base line and apex, then measurement of the peaks width in terms of degree 2°θ have been taken.
6. Refer to Figure 3.4 the observed peaks width have been entered and the average crystallite dimension have been read perpendicular to the refracting plane measured.

Table 3.3 Crystal-size measurements of illite.

Location/Fm/Age	Sample Number	Observed peak width at half heights in degree (2° θ)	Average crystalline size in (A°)
Carboniferous	Ch1	2mm	45A°
	Ch2	3mm	30A°
	Ch4	4mm	45A°
	Ch5	2mm	45A°
	Sa1	2mm	45A°
	Sa2	2mm	45A°
	Sa3	2mm	45A°
	Sa4	2mm	45A°
Permian	Per1	2mm	45A°
	Per2	2mm	45A°
	Per3	2mm	45A°
Triassic	Tr1	4mm	45A°
	Tr2	4mm	45A°
Chukai	Km3	3mm	30A°
	Km4	3mm	30A°

3.4.1.2.3. Interpretation of Results

Results obtained by measurement of illite crystal size show the average particle size of illite range between 25°A and 45°A. The enhanced degree of crystallinity of illite in the samples studied could be related to increasing burrial diagenesis.

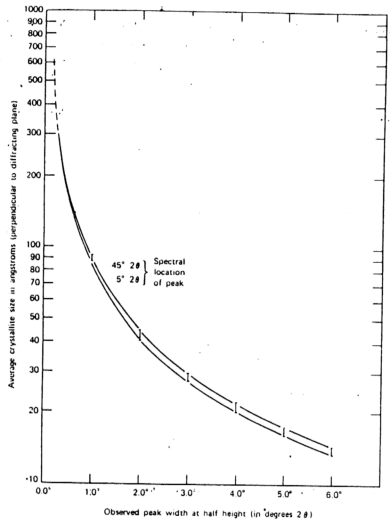

Figure 3.4. Average crystallite size as a function of peak width at half height (After Griffin, 1971).

3.4.2. Kaolinite

Kaolinite has been observed in samples number Tr_1, Tr_2, Per_1, Per_2, Per_3 and Ch_5 in both bulk and clay sized fraction samples. It is represented by their sharp first and third basal reflections on oriented slides respectively. The (001) reflection at 12.2 2θ° 7.17° and (003) reflection at 24.8 2θ° 3.5A°. After have been glycolated and heated to 350° C no changes occur on the two periods of basal reflections, but after have been heated to 550° C, all the reflections completely disappeared. Because at this temperature Kaolinite becomes amorphous to X-ray and it's diffraction pattern disappear (Moor and Reynolds 1989), and also due to a complete dehydration of the Kaolinite see Figures 3.3B, 3.3D, 3.3F.

The X-ray diffractograms of the samples number Ch_1, Ch_2, Ch_3, Ch_4, Sa_1, Sa_2, Sa_3, Sa_4 and Km_1 to Km_{13} show kaolinite present only in minor and trace amounts. The behaviour of the (001) basal reflection of kaolinite can be expressed as shown in Tables 3.4A, 3.4B, 3.4C. The scanning electron micrograph (Plate 3.19) show pseudohexagonal plates of kaolinite. The pseudohexagonal morphology and typical kaolinite EDX spectrum are diagnostic the mineral as kaolinite (see Figure 3.5). The EDX analysis yielding peaks of Si and Al confirmed the identification as kaolinite.

Table 3.4A The behaviour of basal reflection of kaolinite (<2μm) after being treated.

Sample Number	(OO1)			
	Treatments			
	N	GE	350°C	550°C
Ch1	7.1	No	chance	
Ch2	7.1	~	~	
Ch3	7.1	~	~	
Ch4	7.1	~	~	d
Ch5	7.1	~	~	l
Sa1	7.1	~	~	s
Sa2	7.1	~	~	a
Sa3	7.1	~	~	p
Sa4	7.1	~	~	p
Per1	7.1	~	~	e
Per2	7.1	~	~	a
Per3	7.1	~	~	r
Tr1	7.1	~	~	
Tr2	7.1	~	~	

N; normal (Air dried), GE; Glycol ethylene

Table 3.4B The behaviour of (001) basal reflection of Kaolinite after being treated (bulk analysis)

Sample Number	(OO1)			
	Treatments			
	N	GE	350°C	550°C
Km1	7.1	No	change	
Km2	7.1	~	~	d
Km3	7.1	~	~	l
Km4	7.1	~	~	s
Km5	7.1	~	~	a
Km7	7.1	~	~	p
Km8	7.1	~	~	p
Km9	7.1	~	~	e
Km10	7.1	~	~	a
Km11	7.1	~	~	r
Km12	7.1	~	~	
Km13	7.1	~	~	

N; Normal (air dried)

Table 3.4C The behaviour of (001) basal reflection of Kaolinite after being treated (clay-sized fractio)in the Kemaman samples.

Sample Number	(OO1) Treatments			
	N	GE	350°C	550°C
Km1	7.1	No	change	
Km2	7.1	~	~	d
Km3	7.1	~	~	l
Km4	7.1	~	~	s
Km5	7.1	~	~	a
Km7	7.1	~	~	p
Km8	7.1	~	~	p
Km9	7.1	~	~	e
Km10	7.1	~	~	a
Km11	7.1	~	~	r
Km12	7.1	~	~	
Km13	7.1	~	~	

N; Normal (air dried)

3.4.2.1.Kaolinite Crystallinity

The shape of the (001) and (003) basal reflections and intensity can be used to evaluate the crystallinity of kaolinites. Well crystallized kaolinite can be assumed by the presence of narrow, symmetric relatively intense 7A° and 7.5A° reflections (Thorez, 1976). But not well crystallized kaolinite show low intensity and asymmetric (001) and (003) reflections.

Based on the above information both bulk and clay-sized fraction samples in this work show that all samples have asymmetical (001) basal reflection at 12.2 2°θ 7A° toward low angle side, broad and low intensity. All these evidence indicate highly disordered kaolinite which are not well crystallized.

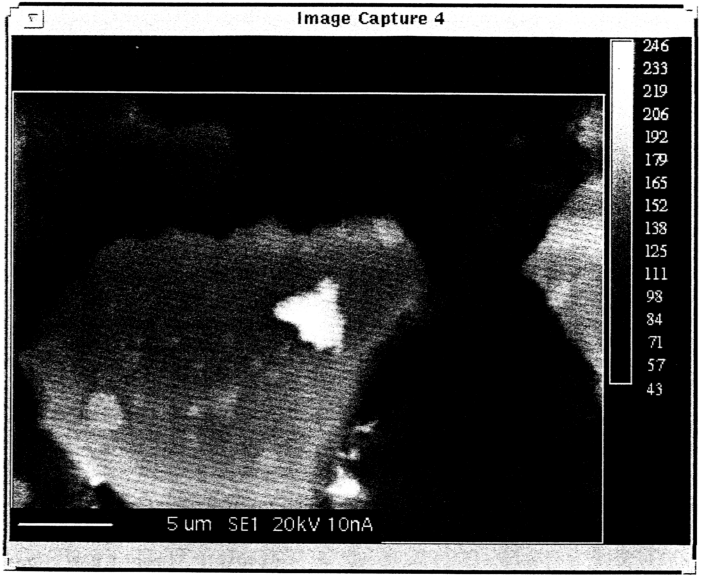

Plate 3.19. Scanning electron micrograph of sample Ch_4 show kaolinite.

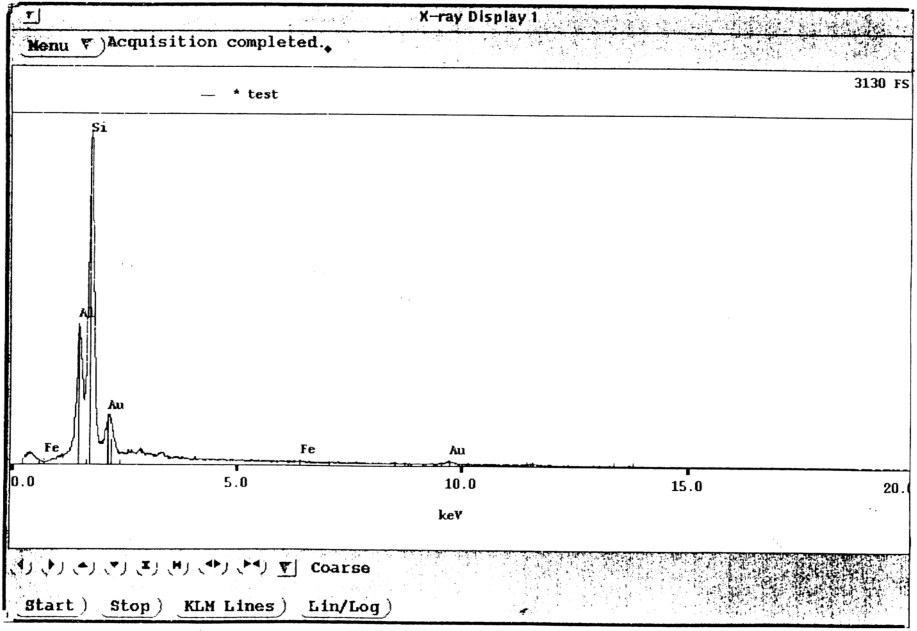

Figure 3.5. Energy Dispersive X-ray spectrum (EDX) of kaolinite, sample Ch_4.

3.4.3. Chlorite

Chlorites exhibit an integral series basal reflections at 14A° (001) and 7A° (002) (Thorez, 1976). But the precise position and intensity of these (001) reflections are deeply depending of the kind of cations occupying both the octahedral and tetrahedral positions. According to the same author the d-spacings are not affected by glycolation or glycerolation. Upon heating to 500 C, the intensites of the (001) reflection are enhanced while it's position is slightly shifted to lower value. Depending upon the above information chlorite mineral observed only in the Kemaman sample (phyllite and slate) and could definitely be identified, it was present in only minor and trace amount as seen in the X-ray diffractograms. The presence of chlorite in small amounts of the samples studied could be related to change in pH of pore water from alkali to acidic condition.

In the Charu, Sagor, Permian and Semantan samples the X-ray diffractograms don't display chlorite. The reason could be related to transformation or destroy chlorite to kaolinite under acidity environment conditions of pore water.

3.5. Pyrophyllite (Pyr)

3.5.1. Introduction

Pyrophyllite is composed of layers structurally similar to micas except it is electrically neutral and it is no interlayer cation (Brown, 1961). The pyrophyllite is an index mineral of very low grade metaclastices of the anchizone, and the low-grade epizone. Pyrophyllite is a relatively rare mineral, and it has a rather layer stability range with respect to pressure (Frey, 1987). Pyrophyllite occurs largely through the hydrothermal alteration of feldspars and is often accompanied by quartz (Deer, et. al.

1962). Pyrophyllite has been regarded as an essentially hydrothermal minerals (Deer, et. al. 1966).

3.5.2. Identification of Pyrophyllite

Pyrophyllite is observed in almost every sample of the Kemaman area, it was recognised on the basis of it is (002) basal reflection at 9.5 2°0 9.3A° and the (004) basal reflection at 19.2 2°0 4.6°A. Both bulk and clay-sized fraction samples after treatment with ethylene glycol and heated at 350°C and 550°C no changes occur on the basal spacing Figures 3.6A, 3.6B, 3.6C, 3.6D. The behaviour of (002) and (004) reflections can be expressed as shown in Table 3.5.

Table 3.5 The behaviour of (002) and (004) basal reflections of Pyrophyllite in the Kemaman samples.

Sample Number	(OO2)				(OO4)			
	Treatments				Treatments			
	N	GE	350°C	550°C	N	GE	350°C	550°C
Km1	9.3	No	changes		4.6	No	changes	
Km2	9.3	~	~		4.6	~	~	
Km3	9.3	~	~		4.6	~	~	
Km4	9.3	~	~		4.6	~	~	
Km5	9.3	~	~		4.6	~	~	
Km7	9.3	~	~		4.6	~	~	
Km8	9.3	~	~		4.6	~	~	
Km9	9.3	~	~		4.6	~	~	
Km10	9.3	~	~		4.6	~	~	
Km11	9.3	~	~		4.6	~	~	
Km12	9.3	~	~		4.6	~	~	
Km13	9.3	~	~		4.6	~	~	

N ; Normal (air dried), GE ; Gylecol ethylene

The presence of pyrophyllite in the Kemaman samples could be related to the hydrothermal alteration of feldspars. However, during Carboniferous age sedimentation continued probably till late Carboniferous, after which the sediments

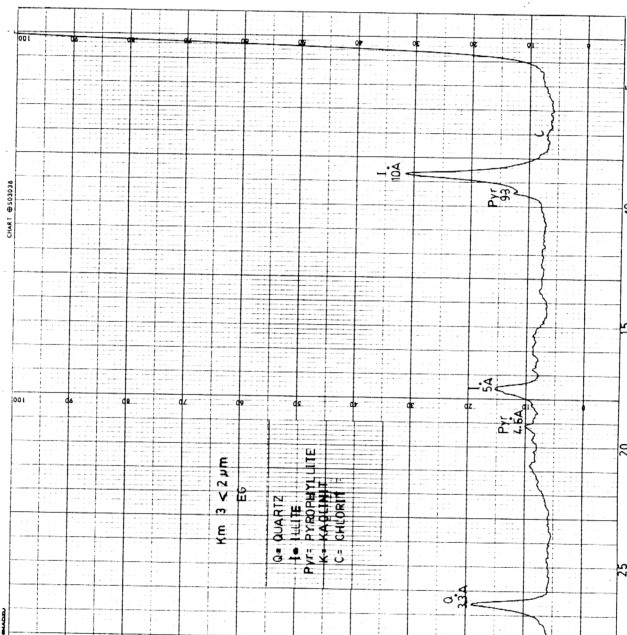

Figure 3.6A. X-ray diffraction pattern of (

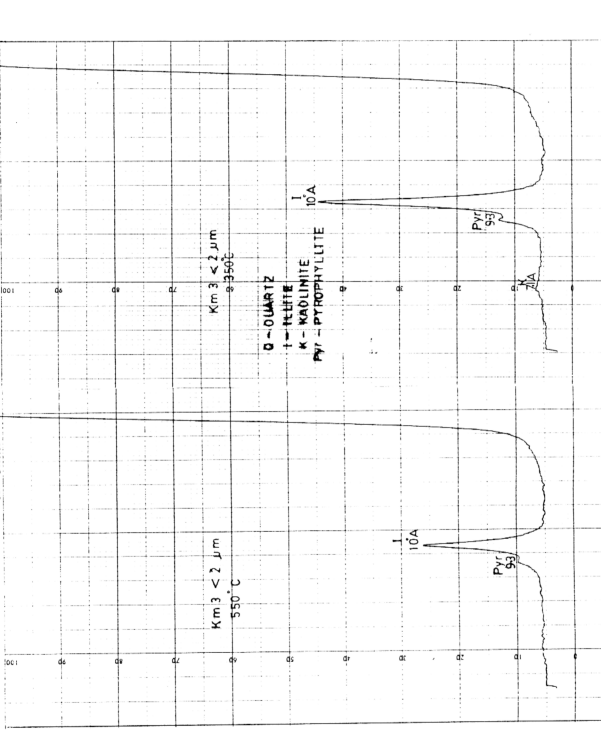

Figure 3.6B. X-ray diffraction pattern of (sample Km_3) after being heated.

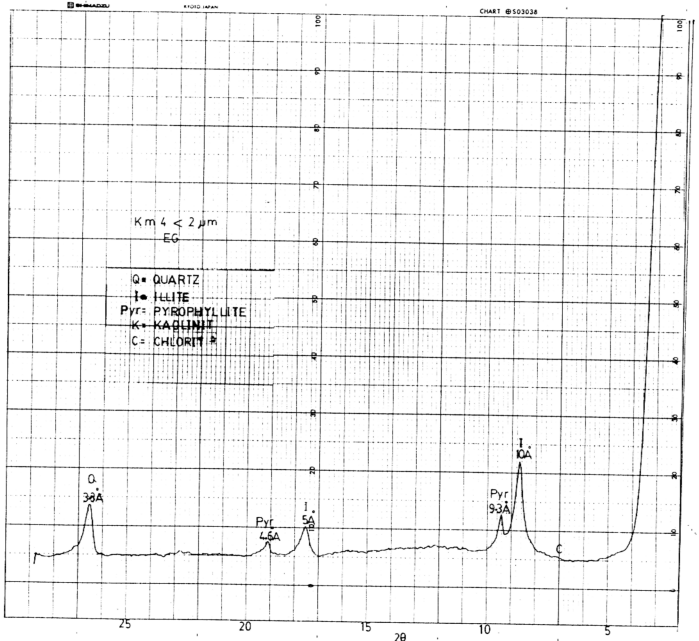

Figure 3.6C. X-ray diffraction pattern of (sample Km4) after being glycolated

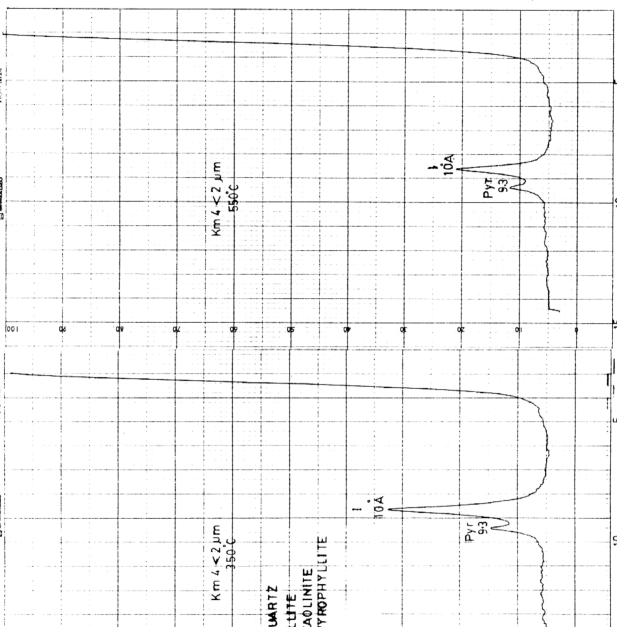

Figure 3.6D. X-ray diffraction pattern of (sample Km_4) after being heated.

suffered intense deformation resulting on isoclinally fold. Igneous intrusion in Triassic age is possible source of thermal metamorphism in the Kemaman, Chukai area. The sediments under went a low-grade metamorphism involving low temperature and confining pressure. Finally under these condition feldspars were altered to pyrophyllite.

The mean vitrinite reflectance % Ro for the Kemaman samples Table 5.1 show the % Ro of the studied samples is in the range of 1.02 – 1.04%. The high % Ro value is being an indication of the increase in thermal maturity. However, correlation between % Ro and presence of the pyrophyllite in the Kemaman samples is observed with vitrinite reflectance data.

3.6. Non Clay Minerals.

Non clay minerals are present often in amounts so small that only their most intense peaks can be seen. These minerals will produce sharp peaks than clay minerals will. The X-ray pattern of bulk samples Figures 3.7A, 3.7B, 3.7C, 3.7D, 3.7E, 3.7F suggest quartz is the most abundant mineral in all the samples studied. It was recognized by very sharp reflections at 26.6 2θ° 3.3A and 20.8 2θ° 4.2A°. Minor amounts of feldspar was detected at 29.8 2θ ° 2.9A° and at 27.82 2θ° 3.2A° in all bulk samples. Dolomite also present in small amounts, it was detected at 31.2 2θ° 2.8A°. Minor amounts of siderite, apatite and anhydrite are present in bulk samples they were detected, at 32 2θ° 2.7A°, at 22.9 2θ° 3.8A° and at 25.4 2θ° at 3.5A° respectively. Muscovite also present in all the samples studied, it was recognized by a very sharp reflection at 35 2 θ ° 2.5 6A °.

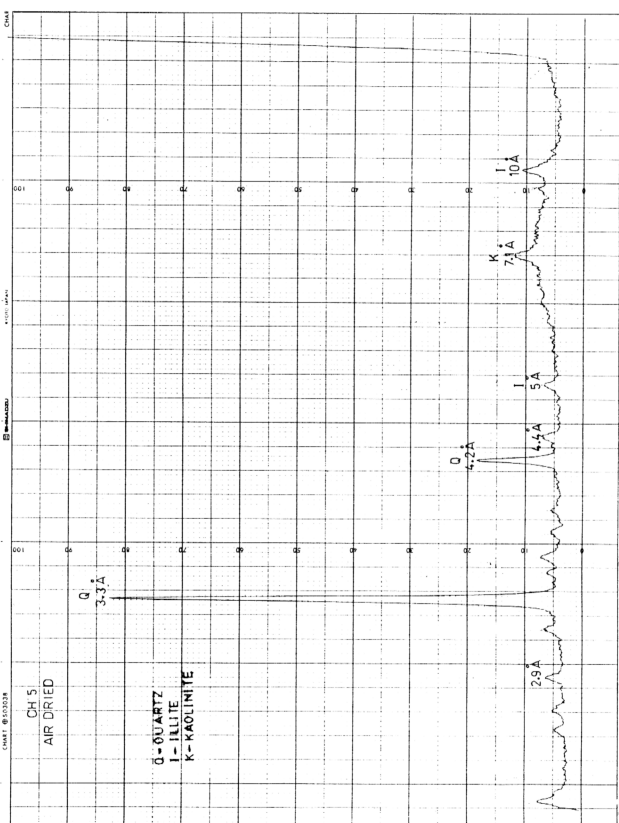

Figure 3.7A. X-ray diffraction pattern of untreated (sample Ch_5) bulk analysis.

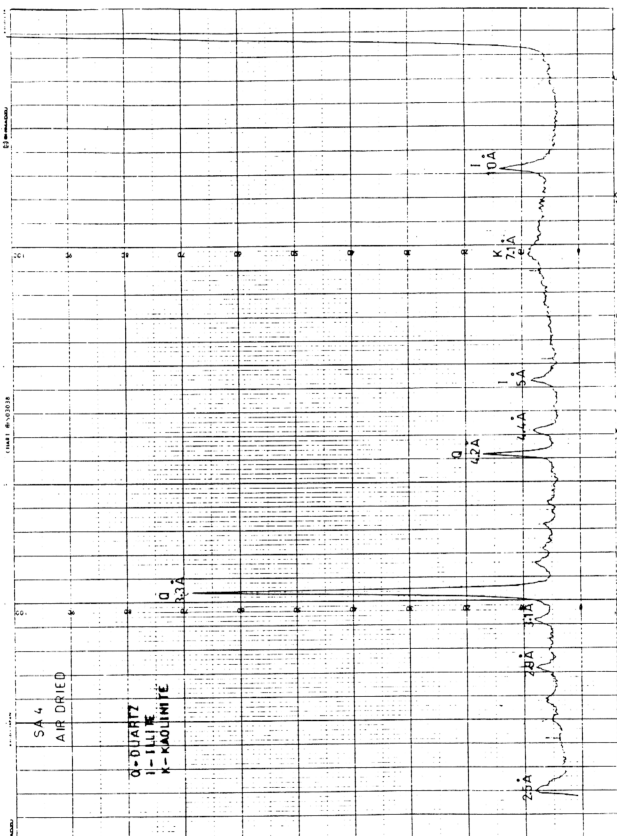

Figure 3.7B. X-ray diffraction pattern of untreated (sample Sa_4) bulk analysis.

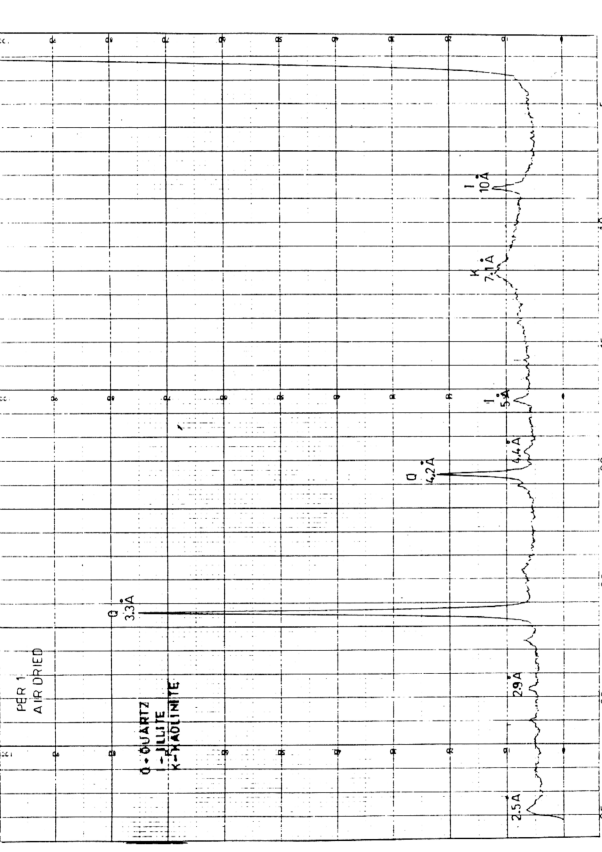

Figure 3.7C. X-ray diffraction pattern of untreated (sample Per_1) bulk analysis.

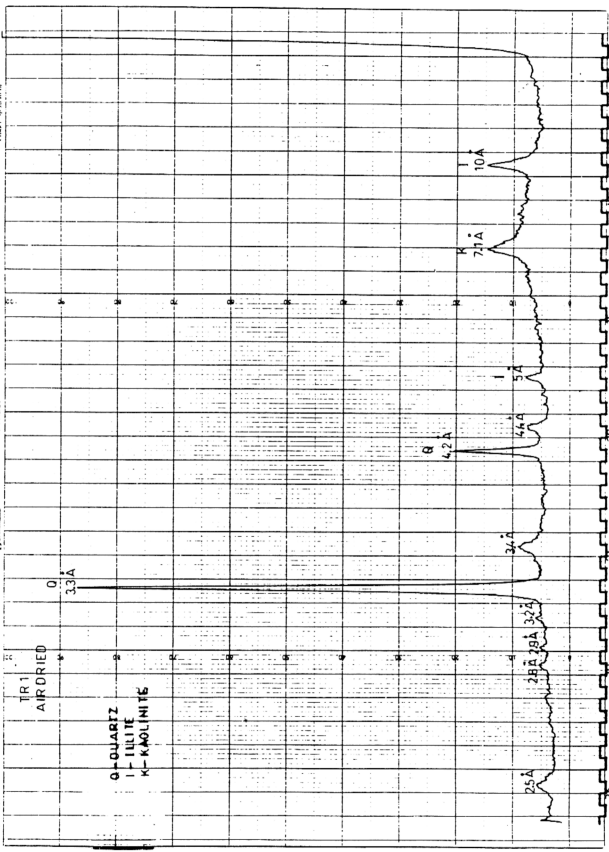

Figure 3.7D. X-ray diffraction pattern of untreated (sample Tr_1) bulk analysis.

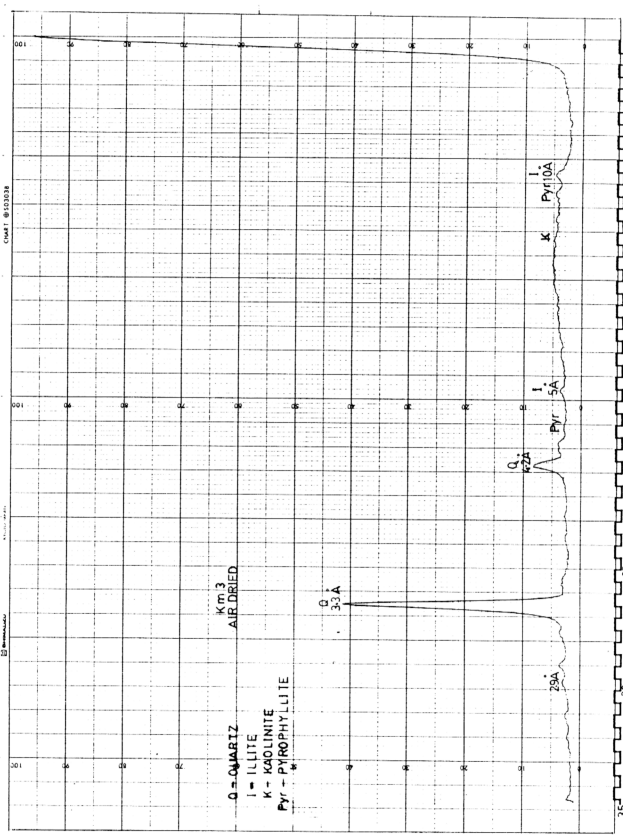

Figure 3.7E. X-ray diffraction pattern of untreated (sample Km) bulk analysis

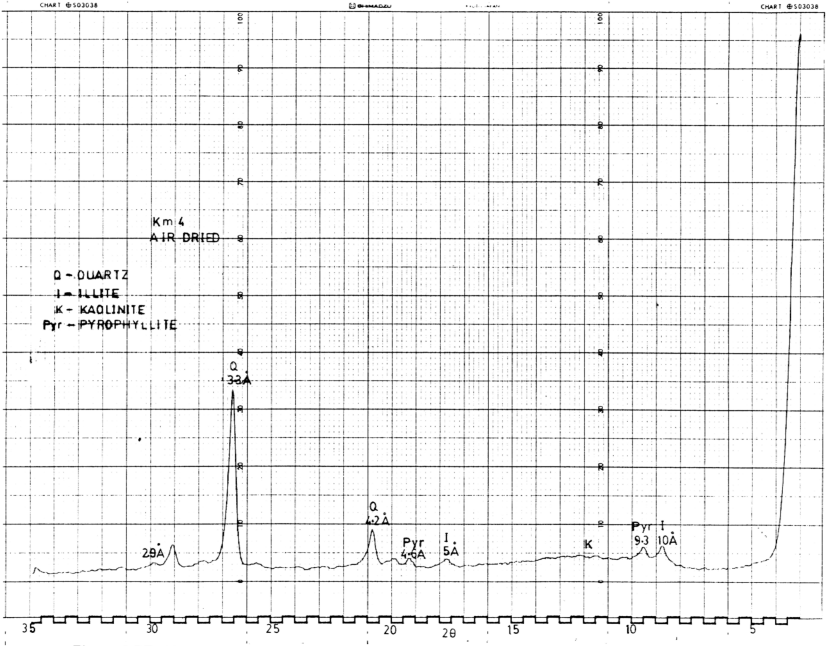

Figure 3.7F. X-ray diffraction pattern of untreated (sample Km_4) bulk analysis of phyllite sample

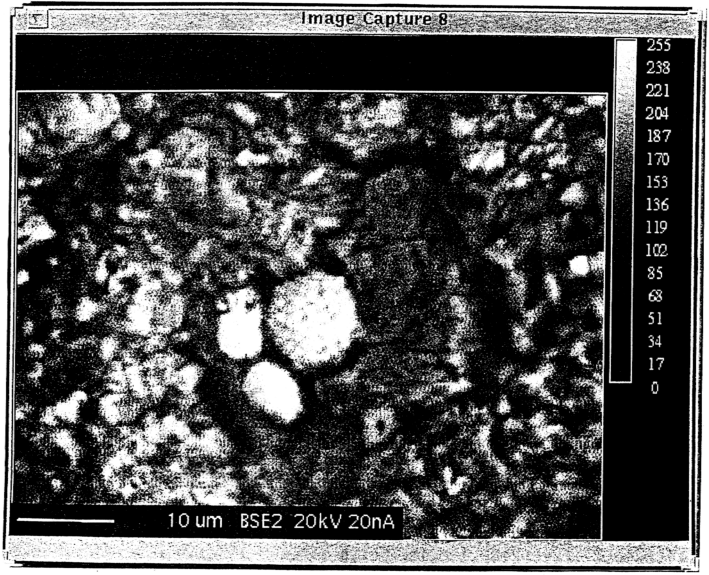

Plate 3.20. Scanning electron micrograph of (sample Per_1) showing framboids pyrite.

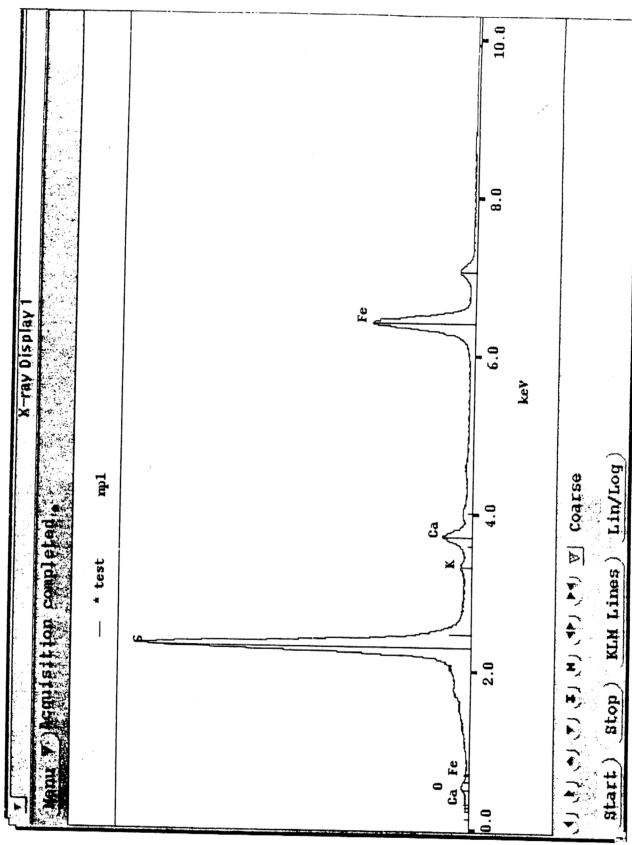

Figure 3.8. Energy Dispersive X-ray spectrum (EDX) of pyrite, sample Per_1.

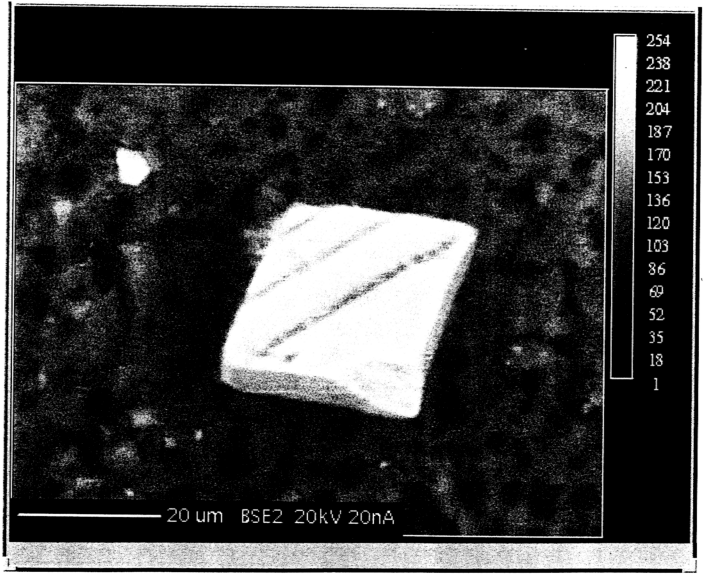

Plate 3.21. Scanning electron micrograph show rhombic morphology of calcite (sample Per_3)

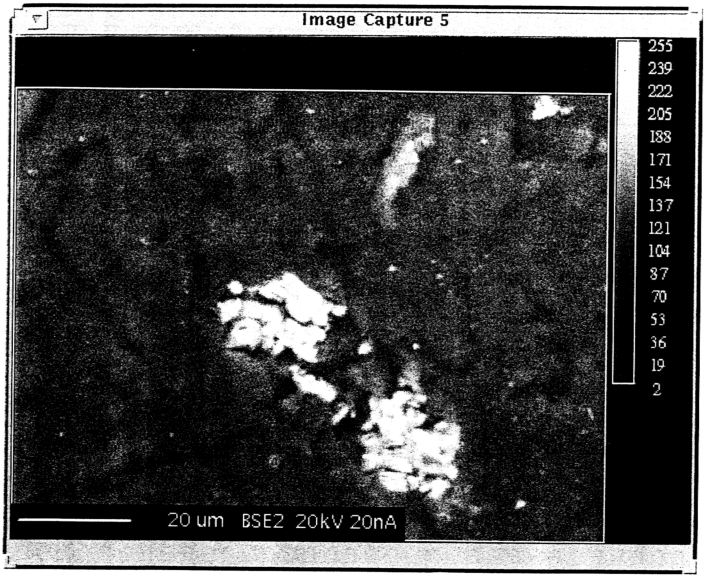

Plate 3.22. Scanning electron micrograph show calcite mineral (sample Per_1).

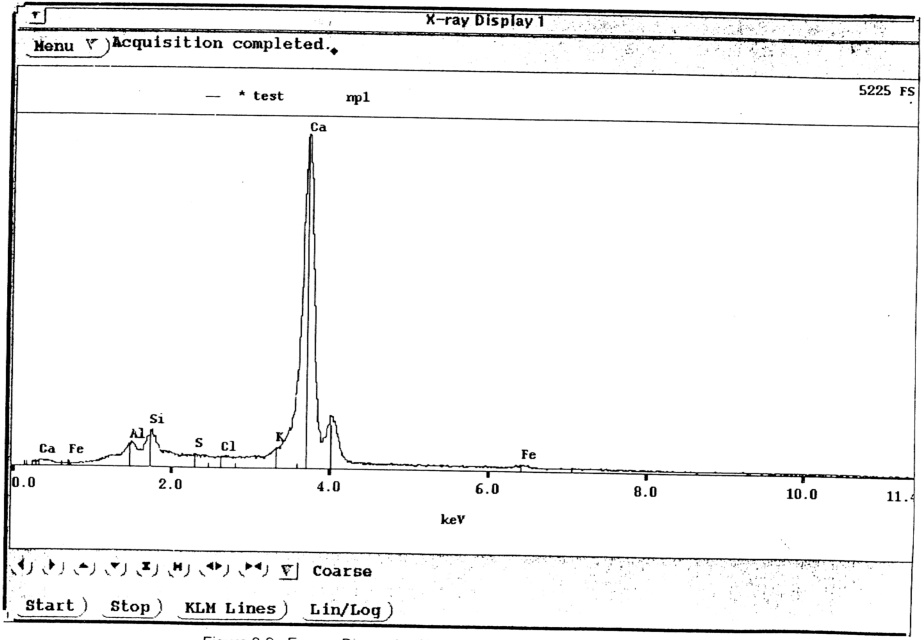

Figure 3.9. Energy Dispersive X-ray spectrum (EDX) of calcite, sample Per_3.

The scanning electron microscope (SEM) photograph (Plate 3.20) show framboid pyrite occurring as aggregates composed of closely packed crystallets. The EDX analysis Figure 3.8 yielding the major elements Fe and S confirming the pyrite identification. The SEM photographs (Plates 3.21, 3.22) also show calcite minerals present in the samples Per1 and Per3. The rhombic morphology and Ca EDX analysis Figure 3.9 were used to identify the crystals as calcite.

3.7. Indicator of Very Low-Grade Metamorphism

Anchizone metamorphism is recognized only on the basis of illite crystallinity data and this method is used as the main indicator of metamorphic grade for very low-grade metaclastic (Frey and Kisch. 1987).

Weaver (1960) was the first to determine relationship between the shape of the illite 10A° diffraction peak and metamorphic grade of shales. He defined a so-called sharpness ratio, that is the intensity ratio at 10.1A° and 10.5A° (Weaver index = H 10.1A°/h 10.5A°). The numerical value of this sharpness ratio increase with enhanced crystallinity, i.e. values less than 2.3 are taken to indicate the diagenetic zone, values from 2.3 to 12.1 the anchzone and values > 12.1 the epizone (Weaver, 1960, Kubler, 1968).

Kubler index is also another method used to identify or investigate low-grade metamorphism. The Kubler index is defined as the half-height peak width of the first illite basal reflection. The numerical values used by Kubler (1984, p, 576) for the limiting of the low grade and high grade of the anchizone are 0.42 and 0.25° $2\Delta\theta$ CuKα. According to Frey (1987), the anchizone is recognized only on the basis of illite crystallinity data, and this method is used as the main indicator of metamorphic

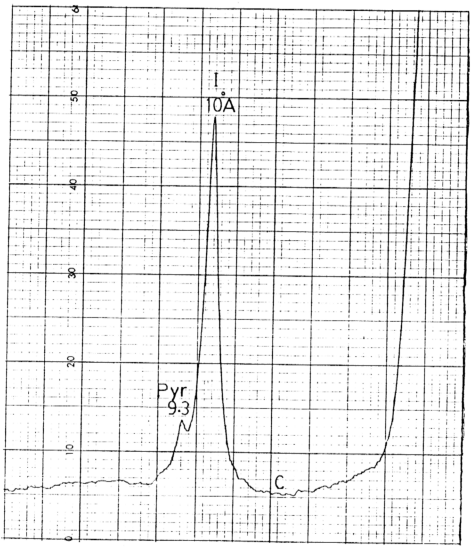

Figure 3.10. First illite basal reflection sample Km_3 (slate).
Location: Bt. Tg. Mat Amin (Chukai).

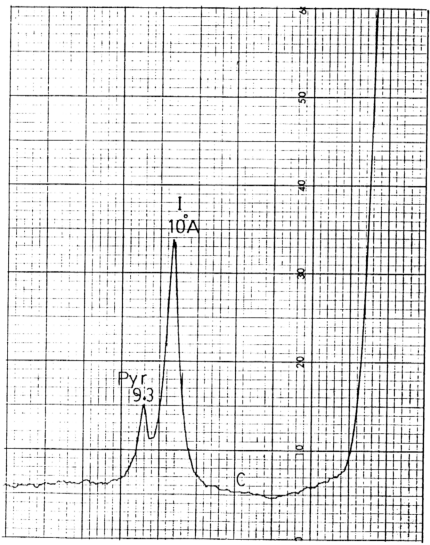

Figure 3.11. First illite basal reflection sample Km_4 (phyllite). Location: Bt. Tg. Mat Amin (Chukai).

grade for very low-grade metaclastics. The anchizone is defined by limiting values of the illite crystallinity index.

The results of the above two methods are given in Table 3.6 and the X-ray diffractograms of the first illite basal reflection of (slate and phyllite) powder samples are shown in Figure 3.10 and 3.11. The 2.4 and 0.42 $\Delta 2°\theta$ and, 3.36 and 0.42 $\Delta 2°\theta$ are the numerical values of illite crystallinity obtained in this work by using Weaver and Kubler indexes methods respectively. The application of the above numerical values of the illite crystallinity have been used here as an indicator of metamorphic grade of very low grade metamorphism of Chukai metasediments.

Base on the above arguments we can say the values obtained from the illite crystallinity of the Chukai samples, Kemaman area indicate that the area suffered regional metamorphism of very low-grade and the illite crystallinity values equivalent to the limits of the anchzone.

Table 3.6 Metamorphic grade for very low-grade metamorphism for Kemaman samples

Sample No.	Weaver indix	Kubler index	Metamorphic Zone	Metamorphic grade
Km3	2.4	0.42 $\Delta 2\theta$	Anchzone	Low-grade
Km4	2.36	0.42 $\Delta 2\theta$	Anchzone	Low-grade

Km3:slate; Km4: phyllite; Location: Bt. Tg. Mat Amin

3.8. Diagenesis

The main objective of this part is used here to shed light on the changes taking place in clay minerals sediments between sedimentation and the completion of

lithification or cementation. Diagenesis that involves changing the composition of the clay minerals requires increase temperature and changeed in pH conditions.

3.8.1 Illite Diagenesis

The illite or hydromuscovite, recrystallized during burial and the gradual transition from a disordered to an ordered composition is seen as a sharpening of the illite peaks for almost every sample studied. Parameters related to this feature can be used as a measure of diagenetic development (Cooper, 1990).

During the burial diagenesis of illite there are possibly two principal pathway. First way in an alkaline environment the illite has been preserved and with increasing burial diagenesis the degree of crystallinity has been enhanced. The second way could be related to a change in pH of pore water from alkali to acidic condition, resulted in illite transformation to kaolinite.

3.8.2. Diagenesis of Kaolinite.

It is well established that burial diagenesis can cause the kaolinite group of mineral to be neoformed, transformed or destroyed. The X-ray diffractograms of the Charu, Sagor and Kemaman samples displayed kaolinite in minor and trace amounts, this could be related to burial diagenesis which caused the kaolinite to be neoformed, transformed, or destroyed, or could be due to the stability of kaolinite which are affected by temperature and pH conditions. The stability of kaolinite mineral in these studied samples could be decrease due to an increase in pH from acidic to alkaline condition with possible transformation of kaolinite to illite if K^+ ion is present.

3.9. Interpretation and Discussion.

Illite associated with quartz is the most widespred clay species supplied by eolian dust in the ocean and some mixed sources supply clay and associate suites in

shallow marine environments (Chamley, 1989). According to the same author suites incorporated in various deposits mostly reflect the detrital sources and can be made to reconstruct environmental and depositional conditions.

Illite and kaolinite are the most abundant clay minerals present in almost every sample analysed for this study. Illite and kaolinite are typical terrigenous species (Chamley 1989). They could be formed by the reworking, without chemical change through simple disaggregation of slate or argillite as indicated by Grim (1968). Illite could be also originated from marine sediment or devided from another illite shales or slate of the source area. In the marine environments illite can form from smecitite following adsorption of potassium and magnesium and collapse of their structure.

According to Folk (1974) illite can be also derived from basic igneous rocks. Kaolinite which is commonly found in the sediments of near shore area can lost and altred to illite or chlorite, it can be also derived from continental or kaolinite source material, it is possible that most parts of illite found in these sediments are from some kaolinite weathering.

Kaolinite could be formed by diagenesis of smectite or chlorite. However if the pH of the pore water are acidic burial diagenesis cause a progressive transformation of smectite and chlorite to kaolinite. According to Tucker (1981) the increase of the depth of burial and metamorphism can modify the nature of clay. The predominent of illite and kaolinite could depend on this factor if we consider that most of the sediments of the area experienced metamorphism. Pyrophyllite could be derived through hydrothermal alteration of feldspars.

3.10. Conclusion

Based on the above arguments the carbonaceous mudstone shales, slates and phyllites of different rock units of the study area could be derived from various source materials including metamorphic, igneous and sedimentary rock fragments.

Illite present in almost every sample of this study, and it is possible that it has been formed from diagenesis, deep burial, and metamorphism. Kaolinite is present in minor and trace amounts in the Charu, Sagor and Kemaman samples.
Chlorite is observed only in the Kemaman Samples (phyllite and slate) and it is present in small amounts. Chlorite could be derived from transformation of smectite during burial diagenesis.

Pyrophyllite detected in every sample of the Kemaman area, and is an index mineral of very low-grade metamorphism. Pyrophyllite is thought to be derived through hydrothermal alteration of feldspars. The clay minerals consist primarly of well-crystallized illite, and disorder kaolinite. Finally illite crystallinity of the Chukai samples indicate that the area was subjected to regional metamorphism of very low-grade equivalent to the limits of the anchizone.

Data such as high % Ro and enhanced the degree of illite crystallinity is being an indication of high thermal maturity, burial diagenesis and metamorphism in all the samples studied. Thus, correlation between the % Ro and enhanced crystallinity is observed with vitrinite reflectance data.